Table of Contents

A Appendix - Impact of climate change Task Force - Convective Weather

In this section of the appendix, we consider both convective storm (i.e., thunderstorm) and one of the phenomena associated with convective storms, hail, in detail. We start with a description of the development of these weather phenomena, we then discuss, both for hail and convective storms, the existing observation data, the proxies used, and we give an overview on the existing literature on projections and highlight knowledge gaps and sources of uncertainty.

The main interest from EASA in this topic stems from projections for the midcentury. However, only a very limited number of studies for that time range has been performed: climate models give a clear picture for the end of the century, but for the midcentury this is less clear, and researchers aim for statistically significant results. Thus, we do not only focus on projections for the midcentury in this appendix.

A.1 Development of Convective Activity and Associated Phenomena

In this subsection, we give a brief overview on the development of convective storms and their associated phenomena. For a more detailed introduction to these processes, we refer to, e.g., [1] [2] [3]. We refer to Figure A.1 and Figure A.2 for illustrations of (some of) the described processes.

Solar radiation heats up the Earth's surface unevenly because of different elevation levels, surface orientation to solar irradiation and different thermal properties of the surface (e.g., a large area of tarmac will heat up more than surrounding grassland). Instability occurs when less dense air with higher temperature than the surrounding parcels is lifted due to the net upward buoyancy force. Apart from local heating, this lifting of air parcels can be triggered by, for example, convergent winds, fronts and orographically driven circulations. The atmospheric conditions that allow the uplifting of air parcels are generally called an *unstable atmosphere*. In the process of rising, the air expands and cools adiabatically following the Dry Adiabatic Lapse Rate (DALR) of 9.8°C every kilometer. The air will continue to rise while the temperature of the air parcel exceeds the temperature of the surrounding air (and starts to sink once the temperature is below that of the surrounding air parcels), where the temperature of the atmosphere decreases with height. These rising masses of air are called thermals, thermal columns, or convective cells. If during the uplift the parcel becomes saturated (in the process of rising and cooling, the air parcel's temperature reaches its dew point and the relative humidity is 100%), the water vapor released from the air parcel condenses into cloud droplets. Hence, a cloud starts to form at that height that becomes the base of a cumulus cloud (lifting condensation level (LCL)). Starting at this point, the rising still cools the air parcel whilst the condensation process releases latent heat and warms the air parcel. Thus, the lapse rate reduces (that is, the air still cools while rising, but in a lower rate) and the air parcel's buoyancy increases. With the rising air and the condensation of water vapor, the cloud grows upwards. Once the temperature of the air parcel drops below the temperature of the surrounding air, the cloud formation stops, and the air starts to sink—a downward flow of air that surrounds the thermal column (which will also happen if the dew point is not reached while rising). The warmer air column that created and sustains the cloud formation is called an updraft/updraught.

If the convective cells grow tall enough (above the zero-degree isotherm), ice crystals will form at the top using ice nucleating particles (INPs), e.g., dust particles, as nuclei. The ice crystals coexist with supercooled cloud droplets, which are very small (with a size range of 10—50 microns to 1 millimeter, typically about 0.02 millimeters). As opposed to larger bodies of liquid water that freeze at 0°C, these microscopical pure water droplets can exist in the liquid state up to -40°C—so-called supercooled water (because they do not have something to freeze onto). The melting level height (MLH) is the altitude at which the temperature is 0°C and ice crystals and snowflakes begin to melt as they descent through the atmosphere. A cumulonimbus cloud has three zones with ice at the top (cooler than -40°C), a mixture of ice and supercooled water below that, and, finally, at the bottom, below MLH, liquid water (warmer than 0°C). When ice crystals from the upper layer drift down (where we have a coexistence of water vapor, liquid water droplets and ice crystals), they grow at the expense of the liquid droplets (Bergeron process [4]). The crystals eventually grow heavy enough to fall to earth because of gravity. When they fall, these ice crystals will often pass the melting level, change phase to liquid, and fall as rain. Another process creates the precipitation in the warmer parts of the cloud: the small cloud droplets bump into each other and coalesce into larger droplets, when these become too large (max 5 millimeters), they break apart because of friction and air resistance into smaller, but still large, rain drops. The precipitation moving downwards drags the air molecules it finds in its path and creates a downward moving draft, the downdraft/downdraught, that comes out from the bottom of the cloud together with the precipitation. As soon as the rain drops leave the cloud, they enter an area with relative humidity below 100%, and evaporation takes place (removing latent heat), and the column of air and rain gets colder and denser. The drier the atmosphere below the base of the Cumulonimbus cloud is, the less precipitation is reaching the ground and the stronger the downdraft is.

A.1.1 Strong Winds in Convective Storms

The evaporation of rain at the cloud base produces cool air, which sinks and then spreads out enhancing the downdraft; this is called a downburst, with the associated cold front referred to as a gust front. This downburst is spreading out from the cloud and encapsulates and eventually disrupts the warm, moist inflow, by which airmass thunderstorm cells cease to exist. However, the outflow may trigger other thunderstorms in the close vicinity of the storm.

The presence of wind shear in the atmospheric profile of the convective environment usually enhances both the intensity and the lifespan of a storm—although it in some cases delays or hinders the initial development of the deep convection. Wind shear is the difference of the surface wind vector to a wind vector higher in the atmosphere (usually the 500hpa level), in magnitude or direction or both. The vertical wind shear yields changes of the storm's structure: the inflow and the outflow (from evaporative cooling) coexist but at two adjacent locations. This results in an organized storm structure and severe long-lived thunderstorms (associated with heavy rains, flooding, hail, lightning, tornadoes, gust-front winds).

A.1.2 Formation of Hail (see [5], [6])

The processes of initiation, growth and melting of hailstones are called microphysical processes. Hailstones grow from hail embryos (ice particles), when these collide with supercooled liquid: the supercooled water freezes onto the hail embryo's surfaces, during which latent heat is released. Thus, the hail embryos growing from collisions with supercooled liquid have a higher surface temperature than the surrounding air. The process of heating up is counterbalanced by cooling from heat transfer to the surrounding air by conduction (and possibly evaporation). There are two mechanisms for growth: the dry and the wet growth.

Dry growth: the main requirement of dry growth is that all accreted mass is either frozen or freezes completely after collection. No vapor diffusion and accretion of liquid (which subsequently freezes) result in latent heat release. For dry growth, the temperature of the ice particle must remain below the freezing point of water so that the surface remains dry (solid ice). The density of the added mass may be at a different density than that of the ice particle. For example, rime density can be as low as 170 kg/m3 or as high as 917 kg/m3 (solid ice).

Wet growth: during wet growth, large ice particles collect significant amounts of supercooled liquid water, some of which does not freeze because latent heat release warms the ice particle to the freezing point. Vapor diffusion and accretion of liquid (which subsequently freezes) result in latent heat release. For wet growth, the latent heat release that results from vapor diffusion and freezing of collected supercooled water is significant enough so that the ice particle's surface temperature rises to 273.15K, the freezing point of water. The unfrozen water can remain on the ice-particle surface, soak porous ice (re-densification), or be shed as droplets. The wet ice surface during wet growth results in efficient ice-ice sticking. This results in efficient mixed-phase growth. Wet growth is most likely for large ice particles in regions with larger liquid water contents (> 1 g/kg) and temperatures above -25°C.

While it is clear that large hailstones cause more harm—for a (spherical) hailstone of diameter d the kinetic energy is approximately proportional to d^4 [7]—the size of a hailstone depends on several factors. In the hail-growth region must be enough supercooled water that the hailstone can collect for it to be able to grow to a large hailstone. Moreover, if we have a high concentration of hail embryos, these compete for the supercooled water and cannot grow into larger hailstones. Additionally, the hailstone must have enough time to grow, and the time increases the stronger the updraught. In addition, the embryo's trajectory must spend as much time as possible in the region of the updraught with a lot of supercooled water [8]. For this, the hailstones fall speed must be at most the speed of the updraught suspending it (if it is above this limit, the hailstone is no longer supported by the storm), and the updraught speed limits the hailstone size. However, if the updraught is too strong, the embryo might get ejected from the growth region, thus, large hailstones are associated with a broad, moderate-strength rotating updraught. Moreover, vertical wind shear influences both the hail embryo and the trajectory within the growth region with high impact of the size of the hailstone. Finally, for hail on the earth's surface, the hailstone size is reduced by the melting below the MLH: small hailstones melt more easily completely until the surface than large hailstones, thus, hailstone sizes distributions (for hailstones reaching the Earth's surface) are shifted towards larger hailstones [9].

If we have many hail embryos that compete for supercooled liquid, but low-strength updraught and little growth time, it is possible to have many small hailstones.

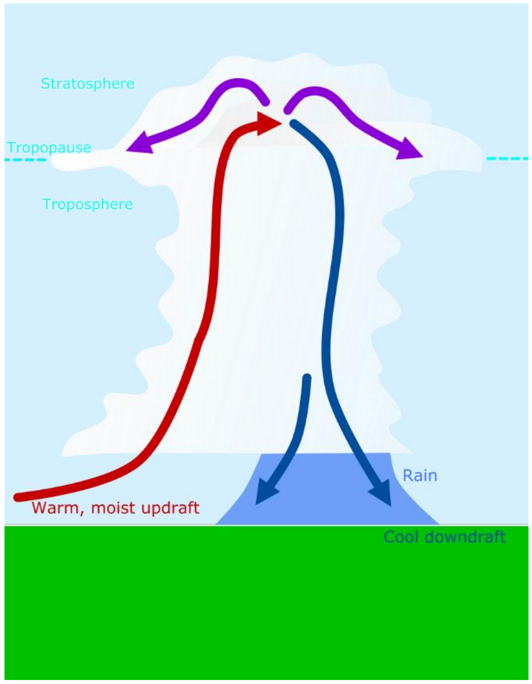

Figure A.1 Updraft, downdraft, and rain in a thunderstorm

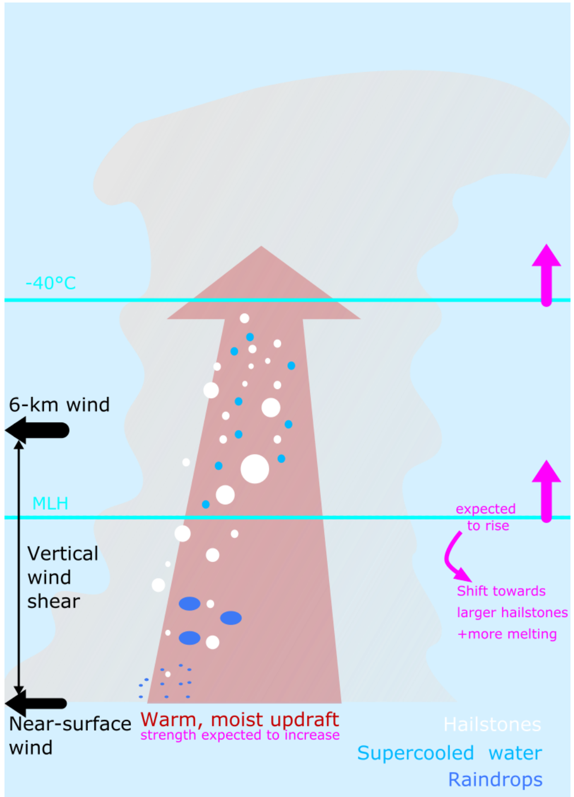

Figure A.2 Hail development and atmospheric phenomena relevant to hail. Expected future changes with climate change are indicated in pink.

A.2 Hail Trends

For hail, in contrast to many other weather phenomena, an overview article by Raupach et al. [5] entitled "The effects of climate change on hailstorms" appeared in Nature Reviews Earth & Environment in 2021. We had meetings with four authors of this study [10] [11], and the paper plus these interviews/discussions build the major foundation for this section.

While several projections for hail in different parts of the world exist, and also some (more or less scarce) observational records (see Section 1.2.1), these usually concern surface hail, that is, the hail that reaches Earth's surface. Hail exceeding a diameter of 2cm when reaching the earth's surface is considered as severe hail.

A.2.1 Past Trends

Hail is small and rare at any given point (in space and time)—it appears during at most 18 days during a year at any given location [10]. Consequently, any observational records are sparse.

Prein and Heymsfield [12], found that during 1979-2010, over land areas the MLH has increased by 32±14 m per decade. This yielded a pronounced melting area. This may explain the shift of the hailstone size distribution towards larger hailstones in China and France [13, 12] and the almost complete elimination of hail events with the concomitant increase in MLH in Colorado.

Past-trend studies are based on observations, hailpads, reports, proxies (e.g., regional climate models, reanalysis data), and indirect observations (e.g., radar, insurance data). Most of these measurements have weaknesses: reports are biased towards population centers; many automatic stations tend to not have any instruments (hailpads etc.) for hail measurements.

Table A.1 Past-trend studies

Geogra-phical area	Geographical restriction	Measurement	Trend
Africa	Northern Algeria, Northern Morocco	Proxies	Positive trend for severe hail in Northern Algeria negative trend for severe hail in Northern Morocco
Asia	China, South Korea, Mongolia, Tibetan Plateau, Northern Caucasus	Observations	Negative trend for China, , South Korea, Mongolia, Tibetan Plateau, Northern Caucasus Positive trend for Northern Caucasus
	Xinjiang, Turkey	Reports	Positive trend for Xinjiang, Turkey
Europe	Romania, Croatia, Serbia, Bulgaria	Observations	Increases in Romania and Croatia, a negative trend in Serbia and Romania, and no trend in Serbia and Bulgaria
	Italy, France, Pyrenees, Greece	Hailpads	No trend in Italy and France, a positive trend for the Pyrenees, and a negative trend for Greece
	UK, Finland, Spain, Europe in general	Reports	positive trend in the UK, Finland, and Europe in general; and no trend for Spain
	Europe in general, Germany, Italy, France, Spain, Eastern Europe	Proxies	Increase for Europe in general (also for severe hail), for Germany, Italy, France, Switzerland, and Spain Decrease for Eastern Europe No trend for Europe in general and for Germany
	Europe, Germany, Greece	Indirect observations	Positive trend for severe hail for Europe and Germany Negative trend for Greece
North America	Alberta, Ontario, Central Rockies,	Observations	Positive trend for Alberta, Ontario, the Central Rockies, the Eastern USA and the High Plains

	Eastern USA, High Plains, Canada, Northern Midwest		No trend for Canada, the Eastern USA, and the Northern Midwest USA Negative trend for the complete USA
	Central and Eastern USA, Western North America	Proxies	Positive trend for the Central and Eastern USA No trend for the complete USA Negative trend for Western North America for severe hail
	Eastern Colorado	Reports	Positive trend for severe hail and no trend otherwise for the complete USA Positive trend for severe hail for Eastern Colorado
		Indirect observations	Negative trend for severe hail and a positive trend otherwise for the complete USA
South America	Argentina, Southern Brazil, Cuyo, Patagonia	Observations	Positive trend for Northwestern and Northeastern Argentina Negative trend for central and eastern Argentina No trend for Southern Brazil, Argentina, Cuyo, and Patagoni
Oceania	Sydney	Reports	Negative trend for Sydney

We will not go in the details of all studies here and refer to [5]; with a list Table A.1 and Figure A.3, we summarize the findings presented by Raupach et al. For several world regions the studies are not consistent and hardly comprehensive. The past-trend studies (usually on hail frequency) show:

- Africa: Proxies indicate a positive trend for the number of severe hail cases in Northern Algeria and a negative trend for severe hail in Northern Morocco
- Asia:
  - Observations indicate a negative trend for hail frequency for China (with a large network), South Korea, Mongolia, the Tibetan Plateau, and the Northern Caucasus; as well as a positive trend for the Northern Caucasus.
  - Reports indicate a positive trend for Xinjiang and Turkey.
- Europe:
  - Observations indicated increases in Romania and Croatia, a negative trend in Serbia and Romania, and no trend in Serbia and Bulgaria.
  - Hailpads indicate no trend in Italy and France, a positive trend for the Pyrenees, and a negative trend for Greece.
  - Reports indicate a positive trend in the UK, Finland, and Europe in general; and no trend for Spain.

- Proxies indicate an increase for Europe in general (also for severe hail), for Germany, Italy, France, Switzerland, and Spain; a decrease for Eastern Europe; and no trend for Europe in general and for Germany.
- Indirect observations indicate a positive trend for severe hail for Europe and Germany, and a negative trend for Greece.

- North America:
  - Observations indicate a positive trend for Alberta, Ontario, the Central Rockies, the Eastern USA, and the High Plains; no trend for Canada, the Eastern USA, and the Northern Midwest USA; and a negative trend for the complete USA.
  - Proxies indicate a positive trend for the Central and Eastern USA, no trend for the complete USA, and a negative trend for Western North America for severe hail.
  - Reports indicate a positive trend for severe hail and no trend otherwise for the complete USA, and a positive trend for severe hail for Eastern Colorado.
  - Indirect observations indicate a negative trend for severe hail and a positive trend otherwise for the complete USA.
- South America: Observations indicate a positive trend for Northwestern and Northeastern Argentina; a negative trend for central and eastern Argentina; and no trend for Southern Brazil, Argentina, Cuyo, and Patagonia.
- Oceania: Reports incidate a negative trend for Sydney.

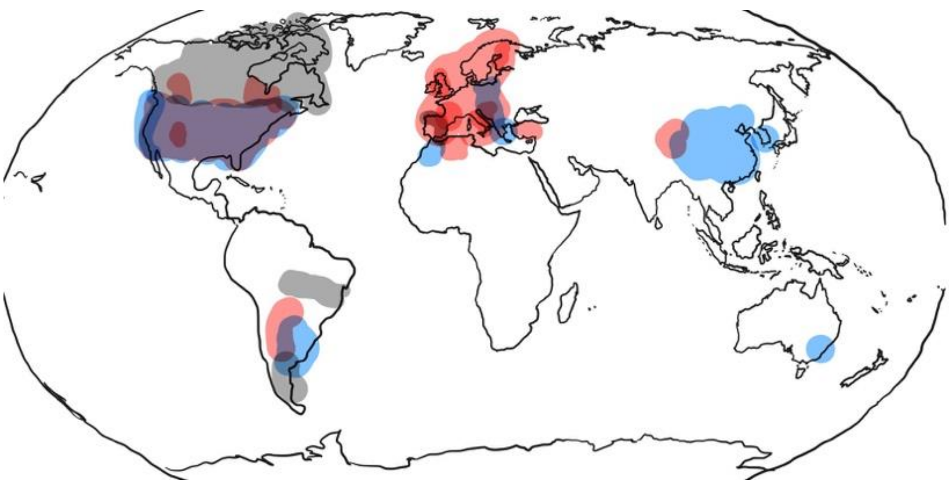

Figure A.3 Hail past trends, blue, red, and gray represent a negative trend, a positive trend, and no trend, respectively.

A.2.2 Proxies for Projections

Most projections are based on proxies, where researchers use:

1. Low-level moisture, convective instability, e.g., convective available potential energy (CAPE). CAPE as a proxy may be misleading since it is the "potential" of instability and in most cases, it is not released into the atmosphere since no initiation occurs. A future increase in CAPE may not lead to subsequent change in the frequency and intensity of severe weather events.
2. Microphysics, mainly MLH.
3. Vertical wind shear (measured as the magnitude of vector difference between the horizontal wind at at surface with a certain atmospheric level. The deep tropospheric wind shear (S06) is defined as the magnitude of the vector difference of the wind at 6km level and to the wind above ground level.)

The National Weather Service [14] defines CAPE as "CAPE or Convective Available Potential Energy is the amount of fuel available to a developing thunderstorm. More specifically, it describes the instability of the atmosphere and provides an approximation of updraft strength within a thunderstorm. "

A.2.3 Projections

The three components that impact hail formation (atmospheric phenomena relevant to hail), are expected to change with climate change [5, 10]:

1. An increase in temperature yields air that can hold more moisture, this Increased low-level moisture yields increased convective instability and updraught strength. Per degree of warming, approximately 7% more tropospheric water vapor is expected [15]. The increased low-level moisture and higher temperatures yield more potential energy, this can be released through condensation of water vapor in a rising air parcel. Hence, this results in increased convective instability [16] [17].
2. For the microphysics, the largest impact is expected to be on the MLH: an increased MLH results in warmer and moister clouds, and possibly more supercooled liquid water, which would yield wet growth of larger hail. The increased MLH yields that more hail will melt into rain before reaching the Earth's surface, which will further shift the distribution of hailstone size towards larger hailstones. However, if we are interested in hail at cruise level (hail aloft), the MLH does not play a role.
3. Overall deep-tropospheric vertical wind shear (S06) is expected to reduce with climate change [18]. However, these changes in vertical wind shear are overshadowed by instability changes, hence, the impact of these vertical-wind-shear changes are expected to be negligible. Here, the interest is not generally on vertical wind shear, but on the vertical wind shear at the time of

thunderstorms. Raupach et al. [5] state "This outcome is because changes to wind shear either occur at times when hail is unlikely to form or are outweighed by the relatively greater effect of changes to instability or MLH. Thus, decreases in wind shear generally do not inhibit expected increases in the occurrence of thunderstorm environments driven by rising convective instability".

Apart from these proxies, there exist direct projections, an example is HAILCAST [19] (based on [20, 7, 21]): a one-dimensional model used in a fine grid, where in each grid cell the growth of a hailstone is projected on a vertical profile. Because these models are one dimensional, they cannot represent the hailstone trajectory in the storm, including the width of the updraft, which play an important role in the growth of hailstones as detailed in Subsection A.1. Brimelow et al. [7] evaluated the performance of HAILCAST and deemed it "a useful aid for objectively forecasting hail" and HAILCAST "being capable of distinguishing between nonsevere- and severe-hail events".

In contrast to HAILCAST, the large-scale proxies only predict favorable conditions, the actual initiation (see a more detailed discussion in Subsection A.3.2) is not clear and the problem of good predictors is highlighted also by proxy-based projections for hail.

Modeling the process of hail formation is computationally expensive, hence, at least until now, these are not fully modelled in projections, and studies that investigate the climate-change impact on these microphysical processes are limited [5].

Many factors of uncertainty exist for the expected changes [10]:

- Trigger mechanisms/initiation not considered in many studies—and even if the atmosphere is prone to produce hail, this still hardly happens
- The microphysical processes of hail are still associated with high uncertainties
- Hail events have high annual variability [22]
- Proxy-based studies have a low resolution, while for the actual formation of hail a high resolution is needed, which in turn are very computationally expensive

The existing future-trend studies are very limited, for an overview see Figure A.4 based on [5], and

Table A.2 (results) and Table A.3 (time frame and models used). We also summarize all results in a list; projections for the midcentury (in contrast to the more frequent end-of-century projections) are highlighted in italics. In particular, the near-future projections show only minor increases or little statistical significance because of high annual variability and ensemble spread.

Table A.2 Future-trend studies for hail: Geographical area, seasonal projections and projections without seasonal distinction. Results for the end of the century are highlighted in gray, results for the middle of the century are highlighted in yellow.

Geogra-phical area	Geographical restriction	Authors/ Reference	Spring	Summer/Warm Season	Without Seasonal Distinction
Europe		Rädler et al. [23]			Frequency of hail will increase
	Germany	Kapsch et al. [24]			7-15% more hail days
	Germany	Mohr et al. [25]		Increasing potential for hail events (in particular: northwest, south of Germany)	
	Italy	Piani et al. [26]			Frequency of hailstorms will increase
	UK	Sanderson et al. [27]			Fewer damaging hailstorms, fewer hailstones of diameter 21-50mm, places where hail appears remains the same
	Netherlands	Botzen et al. [28]			25-50% increase in damage to outdoor farming from hail
North America	Partly central US	Trapp et al. [29]	Increases in very large hail (≥50 mm diameter	Increases in very large hail (≥50 mm diameter	Higher frequency of large hail ((≥35 mm diameter)
	Limited for spring and summer	Brimelow et al. [30]	More hail damage potential over southern North America; Decrease hail frequency and damage potential for eastern + southeastern North America	More hail damage potential over Rocky Mountains; Decrease hail frequency and damage potential for eastern + southeastern North America	Fewer hail days, shift to larger hail sizes
	Colorado	Childs et al. [31]			Increase in hail days
	Colorado	Mahoney et al. [32]		Near-elimination of surface hail	

	Eastern United States	Diffenbaugh et al. [16]			Increase of severe thunderstorm environments that might support formation of hail
	Largest increase for regions close to the Gulf of Mexico and the Atlantic	Trapp et al. [18]		Largest increase	Increase in number of days with severe thunderstorm conditions that support the growth of large hailstones
Oceania	New South Wales	McMaster [33]			Hail losses (not statistically significant)
	Mount Gambier and Melbourne	Niall and Walsh [34]		August-October: increase hail incidence	
	Northern and eastern Australia	Allen et al. [35]			Increase of severe thunderstorm enbironments
	Sydney Basin	Leslie et al. [36]			Increase in frequency and intensity of hailstorms

Table A.3 Future-trend studies for hail: time frame, climate models and emission scenarios considered in the different studies. Results for the end of the century are highlighted in gray, results for the middle of the century are highlighted in yellow.

Geogra-phical area	Geographical restriction	Authors/ Reference	Time frame	Climate models	Scenario, other information
Europe		Rädler et al. [23]	1971-2000 vs. 2071-2100	14 regional climate models (RCMs)	RCP4.5 (emission pathway of stabilization without overshoot) and RCP8.5 (rising emissions pathway)
	Germany	Kapsch et al. [24]	1971-2000 vs. 2031-2045	Eight RCMs	Reananalysis with ERA-40
	Germany	Mohr et al. [25]	1971-2000 vs. 2021-2050	Seven RCMs	
	Italy	Piani et al. [26]	1961-2003 vs. 2004-2040 and 1961-2040	(Use forcings for hailstones from NCEP-NCAR Reanalysis to evaluate expected changes)	Reanalysis and the CGCM2-A2 climate scenario from the Canadian Centre of Climate modeling and analysis
	UK	Sanderson et al. [27]	2010-2039, 2040-2069, 2070-2099	Single RCM	A1B emission scenario (future world of rapid economic growth, balance between all energy sources)

	Netherlands	Botzen et al. [28]	2050	-	Estimate relations between normalized insured hailstorm damage to agriculture and several temperature and precipitation indicators
North America	Partly central US	Trapp et al. [29]	1971-2000 vs. 2071-2100	Global Climate Model (GCM)CM (GFDLCM3 (MIP5)), downscaling	Dynamical downscaling
	Limited for spring and summer	Brimelow et al. [30]	1971-2000 vs. 2041-2070	HAILCAST and one RCM	A2 scenario (describing a heterogenous world and business as usual)
	Colorado	Childs et al. [31]	199 7-2017 vs. 20 71-2100	GCM (GFDLCM3 (MIP5)), dynamical downscaling	RCP8.5 pathway
	Colorado	Mahoney et al. [32]	1971-2041-2070	GCM, RCM	Three-tiered downscaling, explicit simulation of intense thunderstorm events
	Eastern United States	Diffenbaugh et al. [16]	1970-1999 vs. 2070-2099	GCM (GFDLCM3 (MIP5))	RCP8.5 pathway
		Trapp et al. [18]	1962-1989 vs. 2072-2099	Model suite of GCMs and a high-resolution RCM	A2 emission scenario
Oceania	New South Wales	McMaster [33]	1969 vs. 1978	Three GCMs	Doubled-CO_2 scenario; no significant results
	Mount Gambier and Melbourne	Niall and Walsh [34]	1980-2001	August-October: increase hail incidence	Doubled-CO_2 scenario
	Northern and eastern Australia	Allen et al. [35]	1980-2000 vs. 2079-2099	Two GCMs	High-warming climate scenario
	Sydney Basin	Leslie et al. [36]	1990-2002 vs. 2001-2050	GCM (OU-CGCM)	SREAS A1B future climate scenario (future world of rapid economic growth, balance between all energy sources)

- Europe:
  - Rädler et al. [23] showed that the frequency of hail will likely increase by the end of the century. They used an ensemble of 14 regional climate models (RCMs) and showed an increase in likelihood of 40- 80% for environmental conditions favorable for hail in large parts of Europe in a high-emissions scenario—where they perform a comparison of the years 1971-2000 and 2071-2100 and used two benchmark scenarios, so-called

Representative Concentration Pathways (RCPs), RCP4.5 and RCP8.5, where RCP4.5 indicates an emission pathway of stabilization without overshoot and RCP8.5 a rising emissions pathway [37].

  - *Kapsch et al.* [24] *projected a slight increase (7-15%) in the number of hail days in Germany for the period 2031-2045 in comparison with 1971-2000. They used an ensemble of eight RCMs and reanalysis with ERA-40.*
  - *Mohr et al.* [25] *considered the hail frequency in Germany in the summer. They developed a statistical model and by applying it to an ensemble of seven RCMs, they found an increasing potential for hail events for the period of 2021-2050 in comparison to 1971-2000, which is statistically significant for the northwest and south of Germany. However, these projections feature a high variability between simulations.*
  - *Piani et al.* [26] *projected that hailstorm frequency over Italy will likely grow in the future (using reanalysis and the CGCM2-A2 climate scenario from the Canadian Centre of Climate modeling and analysis, CCCma): they compared a reanalysis for 1961-2003 with the CCCma results for 1961-2003, 2004-2040, and 1961-2040. The annual probability of hailstorms will likely increase in the interval 2004-2040, and Piani et al. projected an increase in hail frequency for spring, summer, and autumn.*
  - *Sanderson et al.* [27] *projected a downward trend for the total number of damaging hailstorms for the UK , with statistically significant downward trends for hailstone diameters of 21-50mm.* They projected a decrease for the number of damaging hailstorms by a factor of 2 during the century*. They considered a single RCM and a simple hail-stone formation model, they studied the time periods 2010-2039, 2040-2069, and 2070-2099. Moreover, they found that the spatial distribution did not change: the highest values continued to be in southeast England. This outlier decreasing trend is attributed in a decrease of the CAPE, the climate model's convective instability proxy.*
  - *Botzen et al.* [28] *projected that the annual hailstorm damage to outdoor farming could increase with 25-50% by 2050 in the Netherlands.*

- North America:
  - Trapp et al. [38] projected increases in the frequency of large hail (≥35 mm diameter) over broad geographical areas of the US during all seasons; and increases in very large hail (≥50 mm diameter) for the central US during boreal spring and summer. The authors used high-resolution dynamical downscaling (4 km resolution) to integrate the environmental conditions for and initiation of convective storms that support formation of hail, the storm volume and the depth of the lower atmosphere conductive to melting. They compared the periods 1971-2000 and 2071-2100.

- *Brimelow et al.* [30] *projected fewer hail days over most areas of North America, but a shift toward larger hail sizes, comparing the periods 1971-2000 and 2041-2070. This includes an increase in hail damage potential over southern North America in the spring, and in higher altitudes and the Rocky Mountains in the summer. Moreover, they projected a strong decrease in both hail frequency and damage potential for eastern and southeastern North America in spring and summer (because of increased melting). Generally, drier and cooler regions in North America will experience the largest increased in hail threat, while warmer and more humid regions will experience a reduced threat. The authors used HAILCAST and North American Regional Climate Change Assessment Program (NARCCAP) simulations and the A2 scenario (describing a heterogenous world and business as usual* [39]*).*
- Childs et al. [31] projected an increase in hail days in Colorado by the end of the century based on proxies.
- *Mahoney et al.* [32] *project a near-elimination of surface hail in Colorado during warm season. They attribute this change to an increased MLH. They compare the periods 1971-2000 and 2041-2070. The authors employ a three-tiered downscaling approach: first downscaling GCM simulations to a 50-km grid of NARCCAP RCMs, driven by A2-scneario GCMs; extreme precipitation events occurring in NARCCAP are further downscaled using a high-resolution model with a 1,3-km grid, where intense thunderstorm events can be explicitly simulated.*
- Diffenbaugh et al. [16] projected robust increases of severe thunderstorm environments over the eastern United States based on a GCM ensemble (CMIP5, RCP8.5 pathway). They projected these increases for spring and autumn already before a mean global warming of 2°C. Additionally, they projected an increase in the number of days with high CAPE and strong low-level wind shear—they find decrease in vertical wind shear are concentrated on low-CAPE days and, hence, have little effect. Moreover, they project a shift to high CAPE mostly concentrated on days with low convective inhibition. They mainly compare the periods 1970-1999 and 2070-2099. The authors' criteria for severe thunderstorm environments might support the formation of hail.
- Trapp et al. [18] projected an increase in the number of days in which severe thunderstorm environmental conditions (NDSEV) appear in the US, based on a model suite of GCMs and a high-resolution RCM. The largest NDSEV increases are projected during the summer, for regions close to the Gulf of Mexico and the Atlantic (e.g., >100% increase in Atlanta, GA, and New York, NY). They compare the periods 1962-1989 and 2072-2099. As proxies, they use CAPE and S06. Because large CAPE is associated with strong updrafts, these conditions support the growth of large hailstones; and NDSEV is used as a proxy for thunderstorms that can potentially produce hail.

- Oceania:
  - McMaster [33] used hail-loss models and three GCMs with doubled-CO_2 scenarios to project hail losses for New South Wales. Generally, he obtained declines in winter cereal crop hail losses, but these changes (comparing 1969 and 1978) were not statistically significant.
  - Niall and Walsh [34] considered August-October during the years 1980-2001 in Mount Gambier and Melbourne (both in southeastern Australia) and found a statistically significant relationship between hail incidence and CAPE values for reanalysis data and sounding data. They showed that for a doubled-CO_2 scenario that the mean CAPE decreases by 10%.
  - Allen et al. [40] studied the occurrence of severe thunderstorm environments in Australia using two GCMs, they compared the periods 1980-2000 and 2079-2099 (with high-warming climate scenarios). They projected significant increases of severe thunderstorm environments for northern and eastern Australia—attributed to increasing CAPE, particularly close to warm sea surface temperatures. The authors projected a decrease in frequency of environments with high vertical wind shear, but they predicted that this will be outweighed by the CAPE increase. This result contrasts the changes obtained by McMaster and Niall and Walsh (based on coarse-resolution data).
  - *Leslie et al.* [36] *compared the periods 1990-2002 and 2001-2050 for the Sydney Basin. They used a six-member ensemble of a high-resolution version of the Oklahoma Coupled General Circulation Model with a hierarchy of graded meshes and including cloud microphysics in the 1-km horizontal grid of the model. Under the SREAS A1B future climate scenario (future world of rapid economic growth, balance between all energy sources* [39]*), they obtained significant increase in frequency and intensity of hailstorms in compared both to 1990-2002 and no-change 2001-2050. During the next one or two decades (starting in 2008), the increases in frequency may be masked by natural inter-decadal variability.*

In summary, for Europe, observational trends show little agreement, but a slight increase for environments that are favorable for hail (with low significance and some contradictions, e.g., the UK) is projected. Changes are attributed to more convective instability because of low-level moisture and an increasing MLH. In North America, observations do not show clear trends. However, projections of hail intensity (hail sizes/damaging hail stones) and frequency are consistent between approaches based on different climate models, and an increase of days favoring severe convective storms within most regions and seasons is projected. The changes are attributed on an increase in convective stability, which will outweigh a simultaneous decrease in mean vertical wind shear [16, 18, 38, 41]. The increase in environments is particularly projected for warm seasons and warm and humid regions, the increase in intensity/severity is projected for dry and cool regions, but with fewer events. Altogether a shift to larger hail is projected. For Oceania, projections are scarce, but the existing studies agree in trends: an increase in frequency, severity and favorable environments, but also large inter-decadal variability.

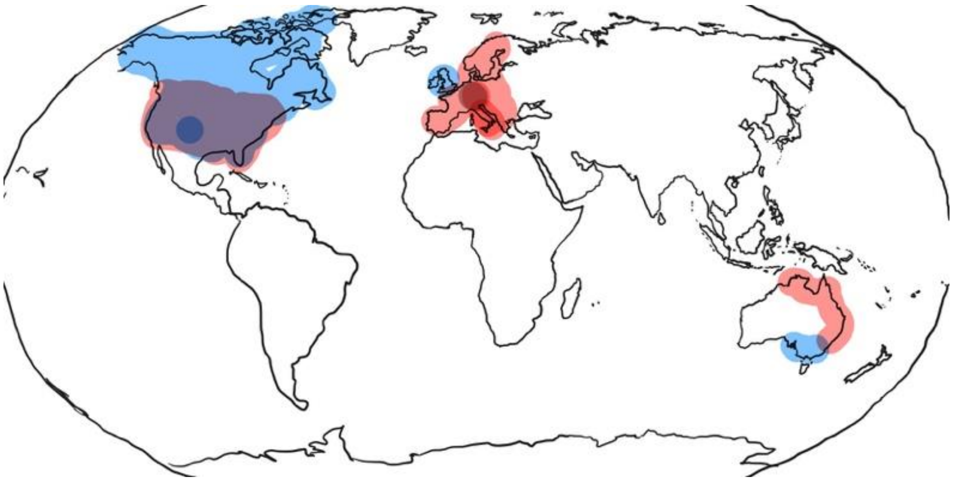

Figure A.4 Hail future studies: blue, red, and gray represent a negative trend, a positive trend, and no trend, respectively.

A.2.4 Knowledge Gaps and Uncertainties

Kunz [10] indicated a lack of data for 500 hPA (about 5000-6000 metres altitude). At 500 hPA—in contrast to 850 hPA, so far only minor temperature trends have been observed.

Figure A.4 clearly indicates large spatial gaps in future studies. However, the same proxies cannot be used for different world regions, e.g., for the UK a completely different method is used than for the rest of Europe. This indicates that the existing spatial gaps (as evident from Figure A.4) cannot be closed by simply using existing proxies.

Uncertainties stem from a variety of factors, as detailed in Subsection A.2.3 [10]:

- Trigger mechanisms/initiation not considered in many studies—and even if the atmosphere is prone to produce hail, this still hardly happens
- The microphysical processes of hail are still associated with high uncertainties
- Hail events have high invariability
- Proxy-based studies have a low resolution, while for the actual formation of hail a high resolution is needed, which in turn are very computationally expensive

Studies on hail aloft (HALO) do not exist but are very interesting for aviation. John T. Allen [11] specifically highlighted the need for EASA to lift this topic to trigger research on HALO.

A.3 Convective Weather (Thunderstorms) Trends

In literature, usually two categories are studied:

- Severe convective storms (SCS)
- Significant severe convective storms (SigSCS)

These include some minimum criteria for associated phenomena, as detailed by Allen [42]:

	SCS	SigSCS
Hail stones diameter	≥ 2cm	≥ 5cm
Winds	≥ 90 km/h	≥ 120 km/h
Tornadoes	Existence	At least F2 intensity[1]
Precipitation (not used in all countries)	Excessive	excessive

For a classification as SCS/SigSCS at least one of these criteria must be met, the strong winds will always be present, while other phenomena may, but need not be present [43]. While the criteria listed here seem to allow for a very clear classification, Allen [42] highlights that “arbitrary criteria […] are used to define [SCS]”, that almost severe and severe thunderstorms are hardly distinguished (there is little physical difference between a near-severe storm with 1.9cm diameter hail and a severe storm with 2cm diameter hail [35] [44]), and that definitions of what constitutes a SCS/SigSCS vary from country to country. For convective storms that do not meet the criteria of an SCS, observational records are not very good.

SCS come with a variety of aviation hazards: hail encounter, lightning strike, low-level wind shear, severe turbulence, runway flooding. In this appendix, we focus on SCS in general and hail, other phenomena are of interest for future reports.

The general expected impact of climate change on convective storms [42] is shown in Figure A.5, however, this includes various uncertain factors, hence, such a clear connection has not been shown in studies.

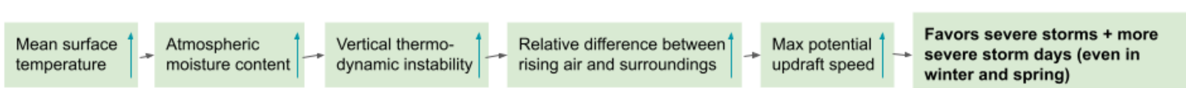

Figure A.5 Expected impact of climate change on severe convective storms

For a more detailed overview on climate change and severe thunderstorms, we refer to the paper of the same name by Allen [42]. This paper and our interview/discussions with the single author of this survey article [11] build the major foundation of this section.

[1] F2 is a measure on the Fujita scale and describes tornadoes with 113-157mph and considerable damage

A.3.1 Observations

There do not exist “reliable, long-term record[s] of severe thunderstorms” [16]. The same restrictions for observations exist as for hail (Subsection A.2.1): observations are skewed towards populations centers (where possible observers are more likely located), surface stations are too scarce. The largest set of records exists for the US, otherwise records are very limited [42]. These factors favor the usage of radar- or satellite-based data, which has fewer spatial limitations, however, it is available for only about the last 10 years.

A.3.2 Proxies for Projections

Environmental proxies should reflect conditions that are favorable for SCS. However, favorable conditions for SCS do not mean that a SCS actually forms, the actual initiation of an SCS is a large problem for projections; Púčik et al. [45] state that “[t]he presence of latent instability does not guarantee that a thunderstorm will form, so that it is not clear whether increases in instability are associated with increases in thunderstorm activity“. Already in 2006, a complete volume of Monthly Weather Review [46] was devoted to convection initiation.

Generally, environmental proxies for three main components are used:

1. Thermodynamic propensity for updraft development, proxies used in literature include:
   a. CAPE
   b. Convective inhibition (CIN)
   c. Lapse rate
   d. Lifted condensation level
   e. Occurrence of convective precipitation
2. Vertical wind shear (to predict the organization and longevity of severe convection of significantly severe convection), proxies used in literature include:
   a. S06
   b. Storm relative helicity (SRH)
   c. Vertical wind shear between surface and lower levels, e.g., S01
3. Convective initiation, proxies used in literature include:
   a. Occurrence of convective precipitation
   b. Boundary-layer convergence zones
   c. Magnitude and depth of lifting at boundaries
   d. Cold-pool strength
   e. Amount of moisture

Many researchers use the product of CAPE and S06. Allen [11] highlighted that many proxies are collinear, hence, the use of proxy does not have a large impact on the results. Moreover, the models used by researchers play a large role for the results because of known biases.

A.3.3 Projections

For two of the three main components listed in Subsection A.3.2 (convective instability and vertical wind shear), the expected changes with climate change as detailed in Subsection A.2.3 hold (increased convective instability, reduced vertical wind shear that is outweighed by the increase in convective instability).

For severe thunderstorms, the same holds as for hail: future studies are very sparce. Diffenbaugh et al. [16] highlight "First, there is no reliable, independent, long-term record of severe thunderstorms—and particularly tornadoes—with which to systematically analyze variability and trends. Second, theoretical arguments and climate model experiments both predict conflicting influences of the large-scale—or "environmental"—conditions that support severe thunderstorms. Third, a suite of processes important for the realization of individual storms in the real atmosphere has remained mostly inaccessible in climate model experiments because of deficiencies in model development and/or computational resources."

Allen [11] described RCMs to be preferable over GCMs because of the spatial resolution.

For an overview of the projections see Figure A.6 based on [5], and in Table A.4 (results) and Table A.5 (time frame and models used). We also summarize all results in a list; again, projections for the midcentury (in contrast to the more frequent end-of-century projections) are highlighted in italics.

Table A.4 Future-trend studies for hail: Geographical area, seasonal projections and projections without seasonal distinction. Results for the end of the century are highlighted in gray, results for the middle of the century are highlighted in yellow.

Geogra-phical area	Geogra-phical restriction	Authors/ Reference	Spring	Summer/ Warm Season	Fall	Winter	Without Seasonal Distinction
Europe	Central and south-central Europe	Púčik et al. [45]					Increase in frequency of unstable environments (robust for end of century, smaller and less robust for middle of century), for middle of century only changes of the Mediterranean coastlines and parts of southeastern Europe robust.
	See the different season results	Marsh et al. [47]	Decrease in mean CAPE, but	Nearly complete CAPE decrease, with an	CAPE increase for the Mediterranean Sea and mainland Europe, as well as a decrease for the	Mean CAPE increase in in the Mediterranean Sea, the	Small increase in favorable environments for severe thunderstorms for most locations in Europe

Geogra-phical area	Geogra-phical restriction	Authors/ Reference	Spring	Summer/ Warm Season	Fall	Winter	Without Seasonal Distinction
			increase on the Faroe Islands	exception of western Norway	Atlantic Ocean and the Faroe Islands	Strait of Gibraltar, the Balearic Islands, southern Italy and the southern Black Sea	
	Iberian Peninsula (often restricted to Mediterranean)	Viceto et al. [48]	Small changes in CAPE; increase in S06	Largest increase in conditions favorable for severe thunderstorms (, mostly for the Mediterranean and its surroundings); Significant increase in CAPE for the Mediterranean; decrease in S06	Large increase in conditions favorable for severe thunderstorms (, mostly for the Mediterranean and its surroundings); Significant increase in CAPE for the Mediterranean; decrease in S06	Small changes in CAPE; increase in S06	
		Rädler et al. [23]					Frequency of convective weather events (lightning, hail, severe wind gusts) will likely increase over Europe. Slight decrease in thunderstorms for southwestern and southeastern Europe.
North America	Eastern US	Diffenbaugh et al. [16]	Increase of severe thunderstorm		Increase of severe thunderstorm environments already before a global warming of 2°C		Increase of severe thunderstorm environments

Geogra-phical area	Geogra-phical restriction	Authors/ Reference	Spring	Summer/ Warm Season	Fall	Winter	Without Seasonal Distinction
			environments already before a global warming of 2°C				
	US Largest increases for regions close to the Gulf of Mexico and the Atlantic	Trapp et al. [18]		Largest increase in NDSEV			Increase in number of days with severe thunderstorm environmental conditions (NDSEV)
	US	Trapp et al. [29]	Decrease in cyclone frequency over the conterminous US			Decrease in cyclone frequency over the conterminous US	Increase in NDSEV
	Northeastern United States, the Great Lakes, and Southeastern Canada	Gensini et al. [41]					Increase in NDSEV
Oceania	Northern and eastern Australia	Allen et al. [35]					Increase of severe thunderstorm environments

Geogra-phical area	Geogra-phical restriction	Authors/ Reference	Spring	Summer/ Warm Season	Fall	Winter	Without Seasonal Distinction
Asia	Japan	Muramatsu et al. [49]	Frequency of strong tornadoes will double	Frequency of strong tornadoes will double on the Japan Sea side of the Japanese Islands			

Table A.5 Future-trend studies for hail: time frame, climate models and emission scenarios considered in the different studies. Results for the end of the century are highlighted in gray, results for the middle of the century are highlighted in yellow.

Geogra-phical area	Geographical restriction	Authors/ Reference	Time frame	Climate models	Scenario, other information
Europe	Central and south-central Europe	Púčik et al. [45]	1971-2000 vs. 2021-2050 and 2071-2100	14 RCMs	RCP4.5 and RCP8.5 emission scenarios
	See the different season results	Marsh et al. [47]	1870-1999 vs. 2000-2099	GCM	A2 emission scenario Compared against NCEP/NCAR Global Reanalysis data
	Iberian Peninsula (often restricted to Mediterranean)	Viceto et al. [48]	1986-2005 vs. 2081-2100	-	RCP8.5 emission scenario ERA-Interim reanalysis MPI Earth System Model
		Rädler et al. [23]	1979-2016	14 RCMs	Statistical model applied to ERA-Interim reanalysis data
North America	Eastern US	Diffenbaugh et al. [16]	1970-1999 vs. 2070-2099	GCM ensemble (CMIP5)	RCP8.5 emission scenario (In reanalysis, CMIP5 did yield too many days with high CAPE.)
	US Largest increases for regions close to the Gulf of	Trapp et al. [18]	1962-1989 vs. 2072-2099	Model suite of GCMs and a high-resolution RCM	A2 emission scenario

Geogra-phical area	Geographical restriction	Authors/ Reference	Time frame	Climate models	Scenario, other information
	Mexico and the Atlantic				
	US	Trapp et al. [29]	1950-2099	5 GCMs	A1B emission scenario (future world of rapid economic growth, balance between all energy sources)
	Northeastern United States, the Great Lakes, and Southeastern Canada	Gensini et al. [41]	1981-1995 vs. 2041-2065	Regional model forced with output from a GCM	A2 emission scenario
Oceania	Northern and eastern Australia	Allen et al. [35]	1980-2000 vs. 2079-2099	2 GCMs	High-warming climate scenarios
Asia	Japan	Muramatsu et al. [49]	1979-2003 vs. 2075-2099	GCM	A1B emission scenario

- Europe:
  - *Púčik et al.* [45] *used 14 RCM covering Europe and the Mediterranean, they considered two climate scenarios (RCP4.5 and RCP8.5* [37]*) and compared the period 1971-2000 to the future periods 2021-2050 and 2071-2100. They projected a robust increase in the frequency of unstable environments in central and south-central Europe for the RCP8.5 scenario and the end of the century. The changes for the mid of the century are smaller and less robust both for the RCP4.5 and the RCP8.5 scenario. The only robust changes for the mid of the century appear for the RCP8.5 scenario (less so for the RCP4.5 scenario) for the Mediterranean coastlines and parts of southeastern Europe. For the midcentury, the ensemble-mean change is ca. 50% of that for the end of the century. Moreover, the authors project small, non-robust changes in the frequency of strong deep-layer shear but identify a decrease in shear for the North of Europe. The authors state "By the end of the century, the simultaneous occurrence of latent instability, strong deep-layer shear, and model precipitation is simulated to increase by up to 100% across central and eastern Europe in the RCP8.5 and by 30%–50% in the RCP4.5 scenario. Until midcentury, increases in the 10%–25% range are forecast for most regions".*
  - Marsh et al. [47] compared the periods 1870-1999 and 2000-2099, using a GCM (Community Climate System Model v3 (CCSM3)) and the A2 emission scenario (and

compared again NCEP/NCAR Global Reanalysis data). The reanalysis showed that the CCSM3 underestimates frequency of severe thunderstorm environments. The authors projected a CAPE increase in winter in the Mediterranean Sea, the Strait of Gibraltar, the Balearic Islands, southern Italy and the southern Black Sea; a spring decrease in mean CAPE—but an increase on the Faroe Islands; a nearly complete CAPE decrease in the summer, with an exception of western Norway; and an autumn CAPE increase for the Mediterranean Sea and mainland Europe, as well as a decrease for the Atlantic Ocean and the Faroe Islands. Altogether, a slight increase in mean CAPE in the cool season and a slight decrease in the warm season. Moreover, they projected little changes in mean wind shear. Thus, the authors projected a small increase in favorable environments for severe thunderstorms for most locations in Europe because of "an increase in the joint occurrence of high CAPE and high deep layer shear". The largest increase was projected for the Mediterranean Sea.

  - Viceto et al. [48] studied conditions favorable to the development of atmospheric stability indices: CAPE, S06 and Severe Weather Threat (SWEAT) for the Iberian Peninsula, comparing the period 1986-2005 with 2081-2100 under the RCP8.5 emission scenario. They projected an increase in CAPE: a significant increase in summer for the Mediterranean and its surroundings; a similar pattern for autumn, but smaller differences; and non-significant differences for spring and winter. They projected an increase in S06 for spring and winter and a decrease for summer and autumn. For the conditions favorable for severe thunderstorms, the authors projected the largest changes in summer (and autumn), mostly for the Mediterranean and its surroundings.
  - Rädler et al. [23] showed that the frequency of convective weather events (lightning, hail, severe wind gusts) will likely increase over Europe by the end of the century. They used 14 RCMs. The increase is attributed to increasing humidity near the earth's surface. They projected a slight decrease in thunderstorms for southwestern and southeastern Europe.

- North America:
  - Diffenbaugh et al. [16] projected robust increases of severe thunderstorm environments over the eastern United States based on a GCM ensemble (CMIP5, RCP8.5 pathway). They projected these increases for spring and autumn already before a mean global warming of 2°C. Additionally, they projected an increase in the number of days with high CAPE and strong low-level wind shear[2]—they find decrease in vertical wind shear are concentrated on low-CAPE days and, hence, have little effect. Moreover, they project a shift to high CAPE mostly concentrated on days with low convective inhibition. They mainly compare

[2] Low-level wind shear is an aviation hazard in itself, however, it was not the focus of this first report, hence, we have not made an extensive literature review on it, and do not report on it separately.

the periods 1970-1999 and 2070-2099. In reanalysis, CMIP5 did yield too many days with high CAPE.
    - Trapp et al. [18] projected an increase in the number of days in which severe thunderstorm environmental conditions (NDSEV) appear in the US, based on a model suite of GCMs and a high-resolution RCM. The largest NDSEV increases are projected during the summer, for regions close to the Gulf of Mexico and the Atlantic (e.g., >100% increase in Atlanta, GA, and New York, NY). They compare the periods 1962-1989 and 2072-2099. As proxies, they use CAPE and S06. They observe an increasing CAPE and a decreasing vertical wind shear, again dominated by the CAPE increase.
    - Trapp et al. [29] projected an increase in frequency of severe-thunderstorm forcing (quantified as NDSEV) for the US and the A1B scenario for greenhouse-gas emissions (future world of rapid economic growth, balance between all energy sources [39]) for the period 1950-2099 based on a five-member ensemble of GCMs. Moreover, they project a decrease in cyclone frequency over the conterminous US in winter and early spring.
    - *Gensini et al.* [41] *projected statistically significant increases in NDSEV in Northeasten United States, the Great Lakes, and Southeastern Canada comparing the periods 1981-1995 and 2041-2065.*
- Oceania:
    - Allen et al. [40] studied the occurrence of severe thunderstorm environments in Australia using two GCMs, they compared the periods 1980-2000 and 2079-2099 (with high-warming climate scenarios). They project significant increases of severe thunderstorm environments for northern and eastern Australia—attributed to increasing CAPE, particularly close to warm sea surface temperatures. The authors project a decrease in frequency of environments with high vertical wind shear, but they predict that this will be outweighed by the CAPE increase.
- Asia:
    - Muramatsu et al. [49] compared the periods 1979-2003 and 2075-2099 under the A1B emission scenario for Japan. They studied strong tornadoes (F2 or greater on the Fujita scale). They projected that the frequency of strong tornadoes will double in almost all of Japan in spring, and on the Japan Sea side of the Japanese Islands in summer. The increase is attributed to an increase in the water-vapor missing ratio and an increase in the temperature in the lower troposphere. (Strong vertical wind shear is again projected to not change or to undergo a slight decrease.)

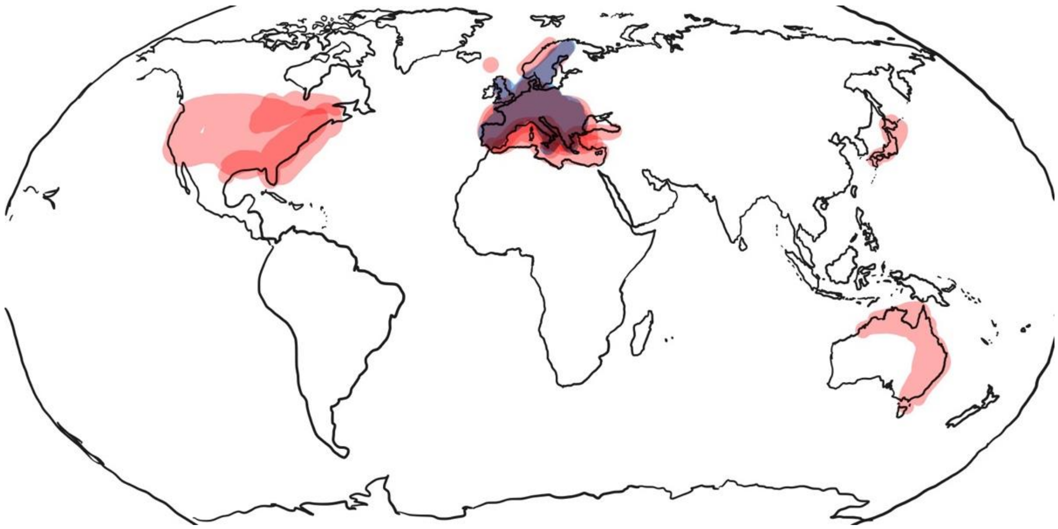

Figure A.6 Severe thunderstorms future studies: blue and red represent a negative and a positive trend, respectively.

Allen [11] highlighted that the cleanest upwards trend can be described for Europe, in particular, for Southern Germany, Italy and Southern France, while he described competing trends for the US. Generally, the trend is more instable, thus, initiated storms tend to be a bigger problem, but they occur less frequently. However, this is not well reflected in climate models.

In summary, for Europe, the frequency of unstable environments is projected to increase for large parts of the continent, with some exceptions, e.g., for southwestern and southeastern Europe. Moreover, researchers project a slight increase in mean CAPE in the cool season and a slight decrease in the warm season—and little changes in mean wind shear. In North America, an increase in the number of days in which severe thunderstorm environmental conditions (NDSEV) is projected—with particularly large increases, e.g., in summer close to the Gulf of Mexico and the Atlantic Ocean. For Australia, significant increases of severe thunderstorm environments for northern and eastern Australia are projected.

A.3.4 Knowledge Gaps and Uncertainties

Similar as for hail, spatial gaps for the future development of severe thunderstorms are evident. Allen [11] underlined that for outside of the USA and Europe no good proxies are known, e.g., the lapse rate in subtropical storms is rarely above 6, while in mid-latitude storms values of 7-9 are common. Even the observational records are temporally and spatially limited.

Moreover, very few authors focus on the middle of the 21st century—the main interest of EASA. The main reason is that statistically significant results can easier be obtained for the end of the century. Hence, to obtain results even for the midcentury, EASA must specifically communicate its interest.

Additionally, the climate models and SCS have different scales: most convective systems have a scale of max 10km and last up to 2-3 hours (but these spatial and temporal limits still allow severe weather phenomena); climate models have a resolution of hundred(s of) km and 6h. These do not match well, and many severe storms cannot be detected by the current generation of climate models. Moreover, in GCMs convective processes are parameterized and storms are not directly simulated. Recently, dynamic downscaling[3] has been used to bridge that gap for simulating future climates. The different resolutions in models may also yield projections that reflect model biases rather than future projections. Given the local properties, Allen [11] estimated downscaling to help with several of the current problems in SCS projections. However, this is currently computationally infeasible.

In addition, many of the phenomena feature large interannual variability. This is most pronounced for tornadoes. This yields the problem of discriminating climate change vs. natural variability.

A major problem when projecting SCS/SigSCS is that different phenomena (wind, hail, tornadoes) are aggregated. However, large hail, damaging winds, and tornadoes are not favoured by the same environmental conditions, which contradicts considering severe thunderstorms as a unified set of hazards.

Finally, environments that are favorable for SCS/SigSCS must not result in a storm, the likelihood for initiation is very local (which is not well reflected in GCMs). Allen [11] described proxies for initiation as nearly stochastic.

A.4 Bibliography

[1] R. B. Smith, *Yale Meteorology,* https://youtube.com/playlist?list=PLkUjvobcQS8YGbXinRsEY_2WabKqrPJ4s, 2013.

[2] M. Strong, "Weather + Climate Lectures," [Online]. Available: melstrong.org/weather-lectures/. [Accessed October 2022].

[3] E. J. Tarbuck, F. K. Lutgens and D. G. Tasa, Earth Science, Pearson, 2015.

[4] G. Richard, "Ch.5 - Bergeron Process & Collision/Coalescence Process," [Online]. Available: https://youtu.be/WByQ3yKxj1s. [Accessed 2022].

[5] T. H. Raupach, O. Martius, J. T. Allen, M. Kunz, S. Lasher-Trapp, S. Mohr, K. L. Rasmussen, R. J. Trapp and Q. Zhang, "The effects of climate change on hailstorms," *Nature Reviews, Earth & Environment,* vol. 2, pp. 213-226, 09 February 2021.

[3] In global climate models, convective processes are parameterized instead of simulating storms directly. Thus, the resolution on SCS is significantly larger than that used in operational weather forecasting. To achieve that granularity even for projections, comparable to high-resolution regional climate models, dynamical downscaling is needed: in areas of interest high resolution is nested with the general low-resolution global climate model. That is, the scale is reduced, but dynamically only in those locations that are of interest for SCS.

[6] H. R. Pruppacher and J. D. Klett, Microphysics of clouds and precipitation, Boston: Kluwer Academic Publishers, 1997.

[7] J. C. Brimelow, G. W. Reuter and E. R. Poolman, "Modeling Maximum Hail Size in Alberta Thunderstorms," *Weather and Forecasting,* vol. 17, no. 5, pp. 1048-1062, 1 October 2002.

[8] E. J. Dennis and M. R. Kumjian, "The Impact of Vertical Wind Shear on Hail Growth in Simulated Supercells," *Journal of the Atmospheric Sciences,* vol. 74, no. 3, pp. 641-663, 2017.

[9] R. Fraile, A. Castro, L. Lopez, J. L. Sanchez and C. Palencia, "The influence of melting on hailstone size distribution," *Atmospheric Research,* Vols. 67-68, pp. 203-213, 2003.

[10] M. Kunz, S. Mohr and T. Raupach, Interviewees, *Hail formation and its impact on climate change.* [Interview]. 10 June 2022.

[11] J. T. Allen, Interviewee, *Impact of climate change on convective activity.* [Interview]. 3 October 2022.

[12] A. F. Prein and A. J. Heymsfield, "Increased melting level height impacts surface precipitation phase and intensity," *Nature Climate Change,* vol. 10, pp. 771-776, 2020.

[13] B. Xie, W. Zhang and Y. Wang, "Trends in hail in China during 1960–2005," *Geophysical Research Letters,* vol. 35, no. 13, 2008.

[14] NATIONAL WEATHER SERVICE, "What is CAPE?," [Online]. Available: https://www.weather.gov/ilx/swop-severetopics-CAPE#:~:text=What%20is%20CAPE%3F,updraft%20strength%20within%20a%20thunderstorm.. [Accessed 28 11 2022].

[15] Intergovernmental Panel on Climate Change, "CLIMATE CHANGE 2013 The Physical Science Basis; Working gorup I contribution to the fifth assessment report of the intergovernmental panel on climate change," Cambridge University Press, 2013.

[16] N. S. Diffenbaugh, M. Scherer and R. J. Trapp, "Robust increases in severe thunderstorm environments in response to greenhouse forcing," *PNAS,* vol. 110, no. 41, pp. 16361-16366, 2013.

[17] K. A. Hoogewind, M. E. Baldwin and R. J. Trapp, "The Impact of Climate Change on Hazardous Convective Weather in the United States: Insight from High-Resolution Dynamical Downscaling," *Journal of Climate,* pp. 10081-10100, 2017.

[18] R. . J. Trapp, N. S. Diffenbaugh, H. E. Brooks, M. E. Baldwin, E. D. Robinson and J. S. Pal, "Changes in severe thunderstorm environment frequency during the 21st century caused by anthropogenically enhanced global radiative forcing," *PNAS,* vol. 104, no. 50, pp. 19719-19723, 2007.

[19] "HAILCAST Homepage," [Online]. Available: http://hailcast.aer.com/. [Accessed 2022].

[20] E. R. Poolman, "Die voorspelling van haelkorrelgroei in Suid-Afrika (The forecasting of hail growth in South Africa)," 1992.

[21] R. Jewell and J. Brimelow, "Evaluation of Alberta Hail Growth Model Using Severe Hail Proximity Soundings from the United States," *Weather and Forecasting,* vol. 24, no. 6, pp. 1592-1609, 2009.

[22] S. Mohr and M. Kunz, "Recent trends and variabilities of convective parameters relevant for hail events in Germany and Europe," *Atmospheric Research,* vol. 123, pp. 211-228, 2013.

[23] A. T. Rädler, P. H. Groenemeijer, E. Faust, R. Sausen and P. Tomáš, "Frequency of severe thunderstorms across Europe expected to increase in the 21st century due to rising instability," *npj Climate and Atmospheric Science,* vol. 2, no. 30, 2019.

[24] M.-L. Kapsch, M. Kunz, R. Vitolo and T. Economou, "Long-term trends of hail-related weather types in an ensemble of regional climate models using a Bayesian approach," *Journal of Geophysical Research,* vol. 117, 2012.

[25] S. Mohr, M. Kunz and K. Keuler, "Development and application of a logistic model to estimate the past and future hail potential inGermany," *Journal of Geophysical Research: Atmospheres,* vol. 120, no. 9, pp. 3939-3956, 2015.

[26] F. Piani, A. Crisci, G. De Chiara, G. Maracchi and F. Meneguzzo, "Recent trends and climatic perspectives of hailstorms frequency and intensity in Tuscany and Central Italy," *Natural Hazards and Earth System Sciences,* vol. 5, pp. 217-224, 2005.

[27] M. G. Sanderson, W. Hand, P. Groenemeijer, P. Boorman, J. Webb and L. McColl, "Projected changes in hailstorms during the 21st century over the UK," *International Journal of Climatology,* vol. 35, no. 1, pp. 15-24, 2015.

[28] W. Botzen, L. Bouwer and J. van den Bergh, "Climate change and hailstorm damage: Empirical evidence and implications for agriculture and insurance," *Resource and Energy Economics,* vol. 32, no. 3, pp. 341-362, 2010.

[29] R. J. Trapp, N. S. Diffenbaugh and A. Gluhovsky, "Transient response of severe thunderstorm forcing to elevated greenhouse gas concentrations," *Geophysical Research Letters,* vol. 36, 2009.

[30] J. C. Brimelow, W. R. Burrows and J. M. Hanesiak, "The changing hail threat over North America in response to anthropogenic climate change," *Nature Climate Change,* vol. 7, 2017.

[31] S. J. Childs, R. S. Schumacher and S. M. Strader, "Projecting End-of-Century Human Exposure from Tornadoes and Severe Hailstorms in Eastern Colorado: Meteorological and Population Perspectives," *Weather, Climate, and Society,* vol. 12, pp. 575-595, 2020.

[32] K. Mahoney, M. A. Alexander , G. Thompson, J. J. Barsugli and J. D. Scott, "Changes in hail and flood risk in high-resolution simulations over Colorado's mountains," *Nature Climate Change,* vol. 2, pp. 125-131, 2012.

[33] H. McMaster, "The Potential Impact of Global Warming on Hail Losses to Winter Cereal Crops in New South Wales," *Climate Change,* vol. 43, pp. 455-476, 1999.

[34] S. Niall and K. Walsh, "The impact of climate change on hailstorms in southeastern Australia," *International Journal of Climatology,* vol. 25, no. 14, pp. 1933-1952, 2005.

[35] J. T. Allen and E. R. Allen , "A review of severe thunderstorms in Australia," *Atmospheric Research,* Vols. 178-179, pp. 347-366, 2016.

[36] L. M. Leslie, M. Leplastrier and B. W. Buckley, "Estimating future trends in severe hailstorms over the Sydney Basin: A climate modelling study," *Atmospheric Research,* vol. 87, pp. 37-51, 2008.

[37] Intergovernmental Panel on Climate Change (IPCC), "Towards New Scenarios for Analysis of Emissions, Climate Change, Impacts, and Response Strategies," Noordwijkerhout, The Netherlands, 2007.

[38] R. J. Trapp, K. A. Hoogewind and S. Lasher-Trapp, "Future Changes in Hail Occurrence in the United States Determined through Convection-Permitting Dynamical Downscaling," *Journal of Climate,* vol. 32, pp. 5493-5509, 2019.

[39] Intergovernmental Panel on Climate Change, "IPCC Special Report Emissions Scenarios; Summary for Policymakers," 2000.

[40] J. T. Allen, D. J. Karoly and K. J. Walsh, "Future Australian Severe Thunderstorm Environments. Part II: The Influence of a Strongly Warming Climate on Convective Environments," *Journal of Climate,* vol. 27, pp. 3848-3868, 2014.

[41] V. A. Gensini, C. Ramseyer and T. L. Mote, "Future convective environments using NARCCAP," *International Journal of Climatology,* vol. 34, no. 5, pp. 1699-1705, 2014.

[42] J. T. Allen, "Climate Change and Severe Thunderstorms," *Oxford Research Encyclopedias, Climate Science,* 2018.

[43] F. Tymvios, *Personal Communication,* 2022.

[44] C. A. Doswell III, "Severe Convective Storms -- an Overview," The American Meteorological Society, 2000.

[45] T. Púčik, P. Groenemeijer, A. T. Rädler, L. Tijssen, G. Nikulin, A. F. Prein, E. van Meijgaard, R. Fealy, D. Jacob and C. Teichmann, "Future Changes in European Severe Convection Environments in a Regional Climate Model Ensemble," *Journal of Climate,* vol. 30, pp. 6771-6794, 2017.

[46] Monthly Weather Review, vol. 134, 2006.

[47] P. T. Marsh, H. E. Brooks and D. J. Karoly, "Preliminary investigation into the severe thunderstorm environment of Europe simulated by the Community Climate System Model 3," *Atmospheric Research,* vol. 93, pp. 607-618, 2009.

[48] C. Viceto, M. Marta-Almeida and A. Rocha, "Future climate change of stability indices for the Iberian Peninsula," *International Journal of Climatology,* 2017.

[49] T. Muramatsu, T. Kato, M. Nakazato, H. Endo and A. Kitoh, "Future Change of Tornadogenesis-Favorable Environmental Conditions in Japan Estimated by a 20-km-Mesh Atmospheric General Circulation Model," *JJaonuuranrayl o2f0 t1h6e Meteorological Society of Japan,* vol. 94A, pp. 105-120, 2016.

[50] J. T. Allen and E. R. Allen.

B Appendix - Impact of climate change TF - Clear Air Turbulence

This section focuses on Clear Air Turbulence, CAT, due to jet streams. Effects due to mountain waves and convection are here disregarded. The investigation has been performed through the interaction with experts (e.g. Paul Williams, Professor of Atmospheric Science, University of Reading, UK and CERFACS, Laurent Terray, Director of the Climate modeling and Global change (GLOBC) Team at CERFACS and PhD Students of the GLOBC Team at CERFACS).

An important source of CAT is strong vertical wind shear, which is prevalent within the atmospheric jet streams (see Fig. B.1). Jet streams are narrow currents of strong wind that generally blow from west to east all across the Earth (zonal flow) and less frequently from northern to southern directions and vice versa (meridional flow). They impact weather, air travel and many other weather phenomena that take place in our atmosphere. They are located close to the tropopause and are generated from strong temperature gradients between air masses with different characteristics. The most common jet streams are found in the cold air-mass adjacent to the polar and the mid-latitude zones (Polar Jet) and the mid-latitude and tropical zones (Sub-tropical Jet). Although not all jet streams have CAT associated with them, there can be significant vertical and horizontal wind shear on the edges of the jet stream, giving rise to sometimes severe clear air turbulence.

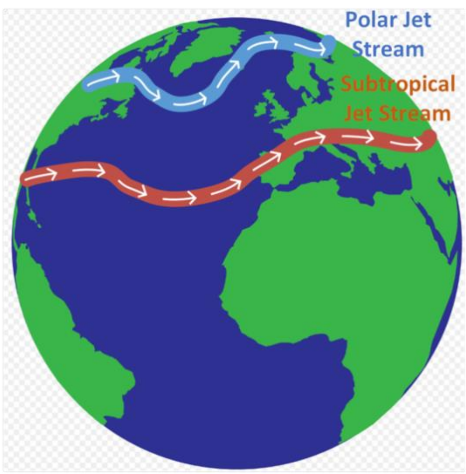

Figure B.1. Jet streams

Stronger jet-stream winds are likely to occur because increased carbon dioxide (CO_2) is enhancing the column-averaged pole-to-equator temperature gradient in the mid-latitudes, through the combined effect of tropospheric warming and stratospheric cooling ([1], [2], [3], see Figure B.2). Climate change is therefore strengthening the wind shear and, consequently CAT is expected to increase in the next decades (see Figure B.3 and Figure B.4).

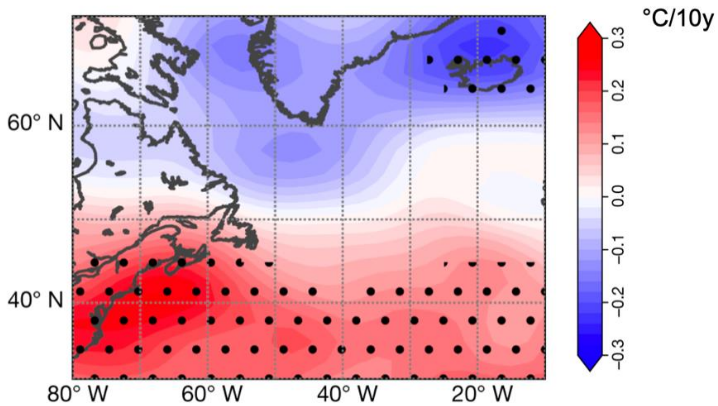

Figure B.2. Observed temperature trends in 1979–2017 at 250 hPa (10000 m, FL 350) in reanalysis data. Results reveal stronger north–south temperature gradient at flight cruising altitudes

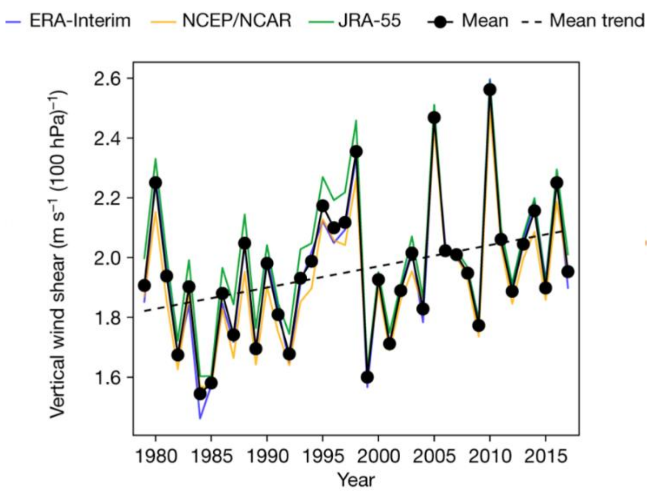

Figure B.3. Observed windshear trends at FL350: annual mean vertical wind shear in North Atlantic at 250 hPa (10000 m, FL 350) calculated with different climate models [4]

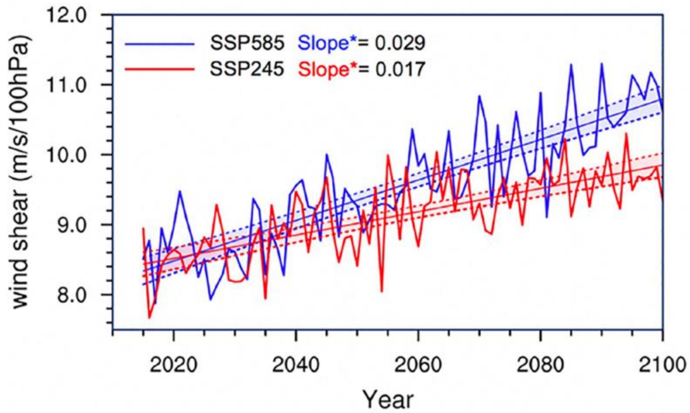

Figure B.4. Projected future windshear trends at FL350 (10000 m): winter mean, CMIP6 (Coupled Model Intercomparison Project) mean vertical wind shear in Northern Eurasia at 250 hPa (blue curve: 29% increase over 85 years; red curve: 17% increase over 85 years).

B.1 Methodology and results

The difficulty in turbulence long-term predictions regarding occurrence of CAT lies largely to the fact that, from the meteorological perspective, turbulence is a “multi-scale” phenomenon. In the atmosphere turbulent “eddies” are contained in a spectrum of sizes, from 100s of kilometers down to centimeters. The effect of the turbulence eddies on aircraft acceleration and trajectory are more pronounced when the size of the eddies is about the size of the aircraft.

While large scale eddies can be predicted, small scale eddies cannot. Fortunately, it appears that most of the energy associated with turbulent eddies on the aircraft scale cascade down from the larger scales of atmospheric motion (e.g., [5] and more recently [6] and [7]), and these larger scales may be resolved by current weather observation networks and numerical weather prediction (NWP) models. Assuming the large-scale predictions are sufficiently accurate, the turbulence prediction problem is then one of identifying large-scale features that are conducive to the formation of aircraft-scale eddies.

The turbulent eddies that cause aviation turbulence typically occur on a reduced set of scales from around 100 m to 1 km. Computer processing speeds are currently not sufficient to explicitly simulate motions on these scales [8], except for a few detailed case studies [9]. Therefore, diagnostic indices from numerical weather prediction models are used to identify and forecast regions likely to contain CAT. The diagnostics indices are mathematical models that generally assume that the smaller-scale turbulence is formed as a result of conditions set by the large-scale flow.

Commonly used indices include:

- variant 1 of the Ellrod and Knapp turbulence index (TI1). The Ellrod–Knapp turbulence index (TI) was developed in the early 1990s and it is in use at many aviation forecasting facilities worldwide. It has been recognized, however, that TI often does not sufficiently account for situations where anticyclonic shear or curvature is present. Variations of the TI that address the weaknesses of the index have been proposed [10] The TI1 variant has been shown to forecast up to 75% of CAT [11].

- the negative Richardson number (−Ri). The Richardson number is the ratio of the stability of the atmosphere (stability suppresses the generation of turbulence) by the turbulence generated by mechanical shear forces at a rate proportional to the square of the acceleration. In essence, the Ri index measures the competition between the destabilizing influence of the wind shear and the stabilizing influence of the stratification of the atmosphere due to density. Strongly negative Richardson numbers indicate that convection predominates, winds are weak, and there is a strong vertical motion characteristic of an unstable atmosphere.
- the Colson – Panofsky index [12]. This index expresses the intensity of turbulence in a sloping baroclinic layer. This index is proportional to the turbulent energy and it discriminates better between regions of varying intensity than vertical wind shear or Richardson number.
- the Brown index (Brown, 1973). The Brown index is a simplification of the Ri tendency equation, originally derived by Roach (1970) [13], relating synoptic scale and mesoscale energetic coupling and gives more information on the relative intensity of these source regions. The simplifications involve use of the thermal wind relation, the gradient wind, as an approximation to the horizontal wind, and some empiricism.
- the potential vorticity, which was found to give unrealistic results. The potential vorticity (PV) is the absolute circulation of an air parcel that is enclosed between two isentropic surfaces. PV consists of two factors, a dynamical element and a thermodynamical element. It is simply the product of absolute vorticity on an isentropic surface and static stability.

Some indices, like the Richardson number, explicitly diagnose a physical mechanism in the atmosphere that is known to cause CAT and are rigorously derivable from the equations of fluid dynamics via a stability analysis. Others, like the Ellrod and Knapp indices, are more empirical.

Then the clear-air turbulence diagnostics are converted into eddy dissipation rates (EDR). The eddy dissipation rate is a natural measure for quantifying the strength of turbulence. For a given aircraft type, aircraft weight, airspeed, and altitude, the root-mean-square vertical acceleration of the aircraft in turbulence is proportional to the cube-root of the eddy dissipation rate [59]. For large commercial aircraft, the correspondence between cube-rooted eddy dissipation rates and turbulence strength categories is shown in Table B.1. In addition, values of cube-rooted eddy dissipation rates of 0.6–0.7 $m^{2/3}\,s^{-1}$ generate severe-to-extreme turbulence, and values greater than 0.7 $m^{2/3}\,s^{-1}$ generate extreme turbulence [9]. For large aircraft, severe air turbulence thus corresponds to $EDR^{1/3}$ higher than 0,5 $m^{2/3}s^{-1}$ and vertical acceleration higher than 1 g, whereas for light aircraft severe air turbulence corresponds to $EDR^{1/3}$ higher than 0,35 $m^{2/3}s^{-1}$ (https://www.aviationweather.gov/turbulence/gt). The threshold EDR value for severe turbulence is aircraft and mission dependent [14]. In contrast the condition of the root-mean-square aircraft vertical acceleration exceeding 1 g is a commonly used definition of severe turbulence for all aircraft.

Turbulence strength category	Null	Light	Light-to-moderate	Moderate	Moderate-to-severe	Severe
$EDR^{1/3}$ range ($m^{2/3}$ s^{-1})	0–0.1	0.1–0.2	0.2–0.3	0.3–0.4	0.4–0.5	>0.5
Vertical acceleration range (g)	0–0.2	0.2–0.4	0.4–0.6	0.6–0.8	0.8–1.0	>1.0
Percentile range (%)	0–97.0	97.0–99.1	99.1–99.6	99.6–99.8	99.8–99.9	99.9–100
Probability (%)	97.0	2.1	0.5	0.2	0.1	0.1

Table B.1: The defining characteristics of six turbulence strength categories for a large commercial aircraft. The eddy dissipation rate and g the acceleration due to gravity. The vertical acceleration assumes proportionality to $DER^{1/3}$, subject the onset of severe turbulence occurring at 1 g. The percentile ranges and probabilities are calculated using an assumed log-normal probability distribution [15].

The log-normal distribution for the cube-rooted eddy dissipation rate yields percentile ranges for each turbulence strength category. These percentile ranges and their corresponding probabilities are listed in Table B.1. The thresholds of the diagnostic indices calculated according to the percentile and probabilities ranges of Table B.1 are listed in Table B.2 [15]. Note that the thresholds are dependent on the grid resolution of the atmospheric model. Therefore, the values listed in Table B.2 may differ from those computed in other studies [8]. The probabilities for each turbulence strength category agree reasonably well with the relative frequencies at which the categories appear in automated in-flight measurements [16] and in PIREPs (Pilot Reports of Turbulence) in the United States [17] and South Korea [18]. Exact quantitative agreement cannot be expected, because of inconsistent PIREP reporting practices and because automated measurements and PIREPs contain a substantial avoidance bias, which is caused by pilots attempting to evade the strongest turbulence [19]. It is then possible to apply the percentile ranges listed in Table B.1 to the probability distributions of the diagnostics indices. By doing so, we may infer the onset threshold for each strength category and each turbulence diagnostic, as shown in Table B.2.

Diagnostic	Units	Light	Light-to-moderate	Moderate	Moderate-to-severe	Severe
Negative Richardson number	—	−15.4	−9.8	−7.9	−6.7	−5.9
Magnitude of vertical shear of horizontal wind	10^{-3} s^{-1}	5.3	6.6	7.4	7.9	8.4
Colson–Panofsky index	10^{3} kt^{2}	−29.3	−27.0	−25.2	−23.7	−22.2
Frontogenesis function	10^{-9} m^{2} s^{-3} K^{-2}	770	1280	1660	1980	2340
Brown index	10^{-6} s^{-1}	99	106	110	113	118
Brown energy dissipation rate	10^{-6} J kg^{-1} s^{-1}	870	1370	1730	2030	2330
Variant 1 of Ellrod's turbulence index	10^{-9} s^{-2}	195	292	360	419	472
Variant 2 of Ellrod's turbulence index	10^{-9} s^{-2}	184	282	356	419	477
Flow deformation	10^{-6} s^{-1}	50.9	60.9	66.9	71.8	76.3
Magnitude of potential vorticity	PVU	8.33	8.73	8.98	9.19	9.41
Relative vorticity squared	10^{-9} s^{-2}	2.46	3.74	4.70	5.50	6.24
Magnitude of horizontal temperature gradient	10^{-6} K m^{-1}	14.7	17.6	19.4	20.8	22.0
Wind speed	m s^{-1}	40.9	48.4	52.4	55.3	58.5
Wind speed × directional shear	10^{-3} rad s^{-1}	3.21	3.94	4.39	4.72	5.08
Flow deformation × wind speed	10^{-3} m s^{-2}	1.65	2.29	2.76	3.17	3.54
Flow deformation × vertical temperature gradient	10^{-9} K m^{-1} s^{-1}	53	84	106	127	151
Magnitude of residual of nonlinear balance equation	10^{-12} s^{-2}	1230	1840	2270	2610	2960
Magnitude of horizontal divergence	10^{-6} s^{-1}	11.9	15.7	18.2	20.4	22.5
Version 1 of North Carolina State University index	10^{-18} s^{-3}	1200	3600	6300	9300	13 000
Negative absolute vorticity advection	10^{-9} s^{-2}	1.33	1.86	2.23	2.56	2.93
Magnitude of relative vorticity advection	10^{-9} s^{-2}	1.44	1.99	2.34	2.66	3.00

Table B.2: Onset thresholds for each turbulence strength category and each clear-air turbulence diagnostic. **The thresholds are for turbulence diagnosed from the GFDL-CM2.1 climate model and apply to large commercial aircraft. In the units column, kt is knots and 1 PVU is 10−6 m2 s−1 K kg−1.**

Figure B.5 shows the results of the analysis of [15], considering the North Atlantic flight corridor as geographic area (50°–75° N, 10°–60°W) at 200 hPa altitude. This geographic area was chosen because the North Atlantic flight corridor is the busiest oceanic airspace in the world. It contains the majority of transatlantic traffic, as indicated by gridded global inventories of fuel burn and emissions obtained from the Federal Aviation Administration's Aviation Environment Design Tool [20], [21], [22], [23]. The analysis refers to winter timeframe (i.e. December, January and February, DJF) because it is the season in which the prevalence of clear-air turbulence peaks in the North Atlantic sector [24]. GFDL-CM2.1 (NOAA Geophysical Fluid Dynamics Laboratory Climate Modeling 2.1, https://www.gfdl.noaa.gov/high-resolution-climate-modeling/) was selected as climate model because the simulated upper-level winds in the northern extra-tropics agree well with reanalysis data, and because the spatial pattern of clear-air turbulence over the North Atlantic diagnosed from reanalysis data is successfully captured by the model [15]. The numerical resolution of the atmosphere is 2.5° in longitude, 2.0° in latitude, and 50 hPa in pressure altitude around the 200 hPa level (12000 m of altitude, i.e. flight level 390). The probability distributions for 21 clear-air turbulence diagnostics are calculated from daily mean temperature and wind fields over 20 winters in each simulation.

The doubled-CO_2 simulation was chosen because the SSP5-8.5 (SSP, Shared Socioeconomic Pathways) scenario of the IPCC Sixth Assessment Report [25] foresees that CO_2 emissions will roughly double from current level by 2050. This is the scenario with very high Green House Gases and CO_2 emissions. Other scenarios with high (SSP3-7.0), intermediate (SSP2-4.5), low (SSP1-2.6) and very low (SSP1-1.9) emissions of Green House Gases and CO_2 are reported in Figure B.6 and in Figure B.7. The IPCC Sixth Assessment

Report did not estimate the likelihoods of the scenarios. The SSP5–8.5 represents the high end of the range of future pathways, corresponding to RCP 8.5 (Representative Concentration Pathways).

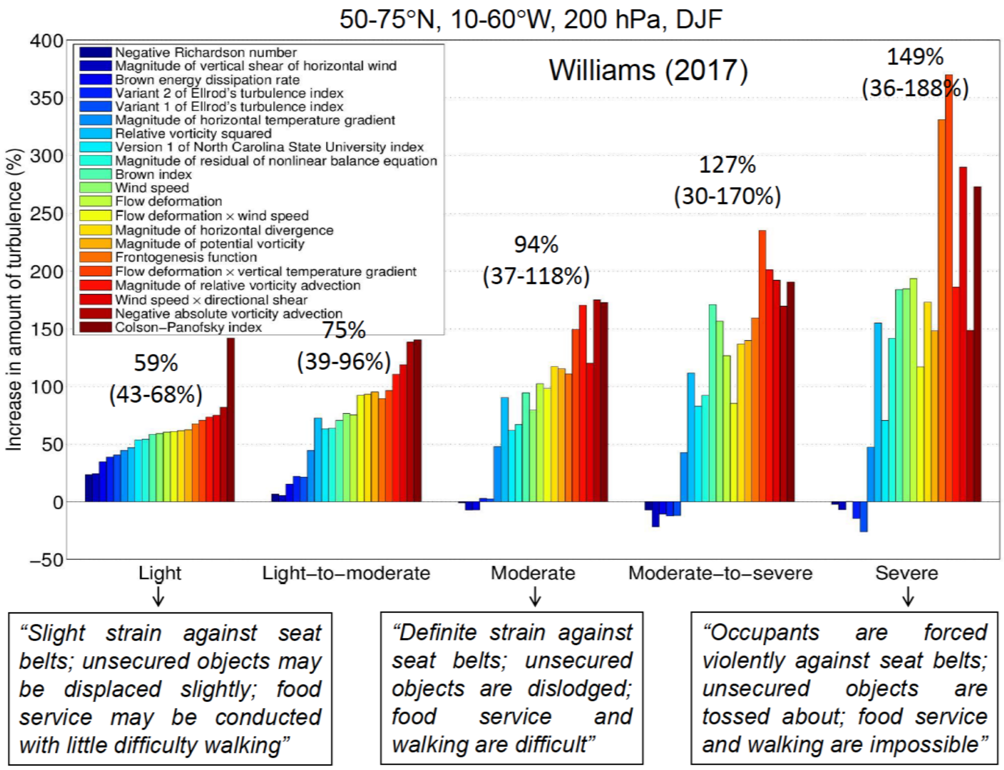

Figure B.5. **Bar charts showing the percentage increase in the amount of light, light-to-moderate, moderate, moderate-to-severe, and severe CAT within the North Atlantic flight corridor at 200 hPa (12000 m) in winter. The increase refers to the change in a doubled-CO_2 simulation compared to a pre-industrial simulation [60] in a time horizon of 20 years, 2050-2070.**

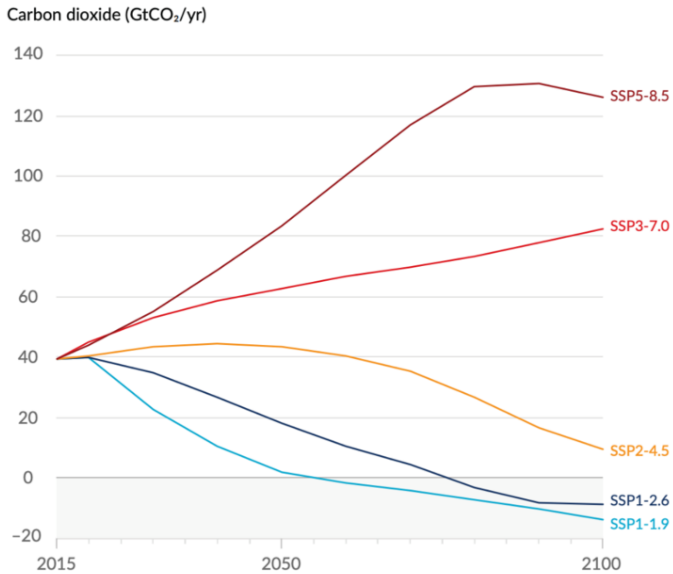

Figure B.6. Future annual emissions of CO_2 across five illustrative scenarios [25]

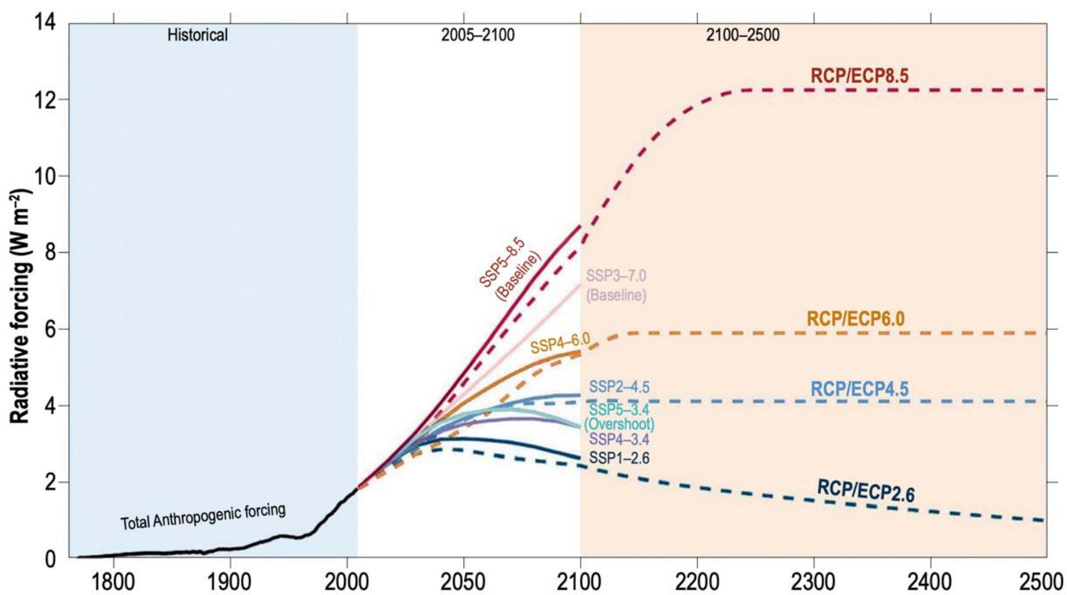

Figure B.7. Radiative forcing (Wm^{-2}) time series for historical data (1765–2004), and for future scenarios from the Representative Concentration Pathways (RCP; 2005–2100) and their continuation as the extended RCPs (2100–2500), and the Shared Socioeconomic Pathways (SSP; 2005–2100). The RCP scenarios are shown as dashed curves, and SSPs are shown as solid curves [26]

The probability gains, expressed as percentage increases in the doubled-CO_2 climate relative to the pre-industrial climate, are shown in Figure B.5 per turbulence diagnostic and strength category. Specifically, all 21 diagnostics show increases in the amount of light and light-to-moderate turbulence, and at least 16 of the 21 diagnostics show increases in the amount of moderate, moderate-to-severe, and severe turbulence. To summarise, the 21 different estimates of the percentage increase within each strength category, the median (50th percentile) and 25th–75th percentiles have been calculated, which respectively indicate an ensemble-average value and an intra-ensemble range. By these measures, the prevalence of:

- light turbulence increases by 59% (43%–68%)
- light-to-moderate increases by 75% (39%–96%)
- moderate increases by 94% (37%–118%)
- moderate-to-severe increases by 127% (30%–170%)
- severe increases by 149% (36%–188.

The averages and ranges both increase substantially from light to severe turbulence, suggesting greater percentage increases in stronger turbulence than weaker turbulence, but also implying a higher degree of uncertainty.

In [27] the probability distribution is calculated for 20 CAT diagnostics from 6-hourly global fields over 30 years (2050-2080) run of the HadGEM2-ES climate model (Hadley Centre Global Environment Model version 2 climate model, https://www.metoffice.gov.uk/research/approach/modelling-systems/unified-model/climate-models/hadgem2) in all seasons at both 200 hPa and 250 hPa, which correspond to typical cruising altitudes of approximately 12 km (39 000 ft or FL390) and 10 km (34,000 ft or FL340), respectively. The HadGEM2-ES climate model forms part of the fifth Coupled Model Intercomparison Project (CMIP5) ensemble [28]. The atmosphere model has a horizontal grid spacing of 1.25° in latitude and 1.875° in longitude, which is finer than the 2.0° by 2.5° GFDL-CM2.1 model used by [15] and [29]. Two HadGEM2-ES simulations are analyzed to calculate how climate change could impact CAT in the upper troposphere and lower stratosphere in future: 1) a preindustrial control simulation (picontrol); 2) a climate change simulation using the Intergovernmental Panel on Climate Change (IPCC) Representative Concentration Pathway 8.5 (RCP8.5, which corresponds to the worst-case climate change scenario or SSP5-8.5, see Figure B.6 and Figure B.7) [25], [26], [30]. The picontrol run is a base state that uses constant preindustrial greenhouse gas concentrations to simulate the global climate before the industrial revolution. The RCP8.5 run assumes a net radiative forcing increase of 8.5 Wm^{-2} by 2100 [26], [31] which implies greenhouse gas concentrations equivalent to around 1370 ppmv of CO_2.

Figure B.8 reports the comparison of the results of the HadGEM2-ES simulations from [27] with the GFDL-CM2.1 simulations from [15]. The CAT increases in HadGEM2-ES are on average 30% smaller than in GFDL-CM2.1, possibly because of the different anthropogenic forcing used in the climate change simulations. Specifically, the GFDL-CM2.1 climate change simulation was allowed to equilibrate after the CO_2 loading had been instantaneously doubled. In contrast, the HadGEM2-ES climate change simulation was a transient RCP8.5 run in which the radiative forcing was gradually increased, and so the atmospheric circulation is not expected to be in equilibrium with the contemporary radiative forcing. Therefore, the comparison is not strictly like for like. The comparison shows for the first time that the projected increase in transatlantic turbulence is robust: it occurs across multiple climate models; it does not depend on the parameterized physics, model resolution, or greenhouse gas scenario.

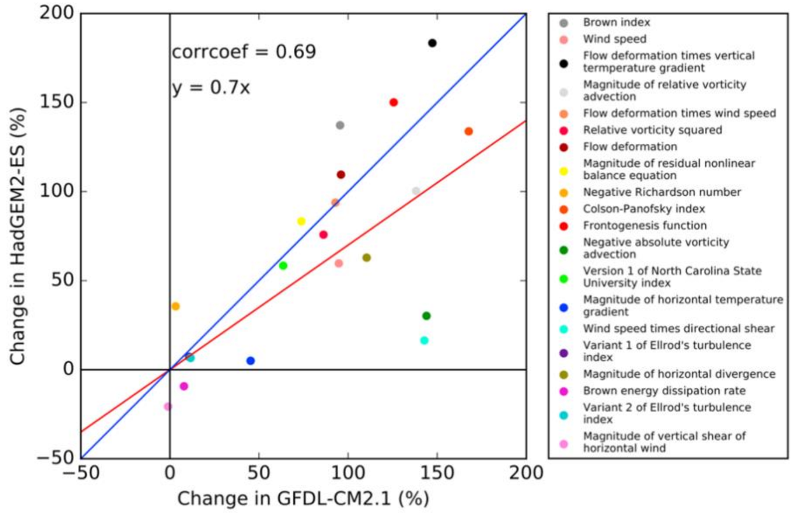

Figure B.8. Scatterplot comparing the HadGEM2-ES simulations from [27] with the GFDL-CM2.1 simulations from [15]. The plot shows the percentage change in the prevalence of moderate-or-greater (MOG) turbulence for 20 CAT diagnostics calculated at 200hPa (12000 m of altitude) over the North Atlantic (50-75° N and 10-60° W) in winter (December, January and February, DJF). The blue line (y=x) indicates parity and the red line (y=0,7x) is a least-squares fit constrained to pass through the origin.

As far as the magnitude of moderate turbulence with respect to coverage, results [27] reveal that in the tropical regions (30°S–30°N), the percentage changes are generally smaller if compared with middle and high latitudes regions because CAT is not a major hazard in the tropics, where convective turbulence dominates. This is indeed because the main jet streams are extra-tropical. Moreover, it is worth underlying that in the tropical regions there is less agreement between the diagnostics, while in the middle and high-latitude regions there is more agreement between the diagnostics because CAT diagnostics were developed to diagnose and predict mid-latitude CAT near jet streams, so they are optimised to be skillful for these regions rather than the tropics. The percentage change in the amount of moderate CAT from preindustrial times (picontrol) to the period 2050–2080 (RCP8.5) at 200 hPa are calculated for all 20 CAT diagnostics in December, January, and February using the HadGEM2-ES climate model. The seven GTG upper-level CAT diagnostics that are used operationally to forecast CAT in the short-term are included in the overall 20 CAT diagnostics. The GTG2, Graphical Turbulence Guidance, the original Integrated Turbulence Forecasting Algorithm (ITFA) then renamed GTG, is a completely automated turbulence forecasting system, developed and tested by the Research Applications Laboratory at the National Center for Atmospheric Research (NCAR/RAL) and the National Oceanic and Atmospheric Administration's (NOAA) Earth System Research Laboratory/Global Systems Division (NOAA- Research-ESRL/GSD), under sponsorship from the FAA's Aviation Weather Research Program).

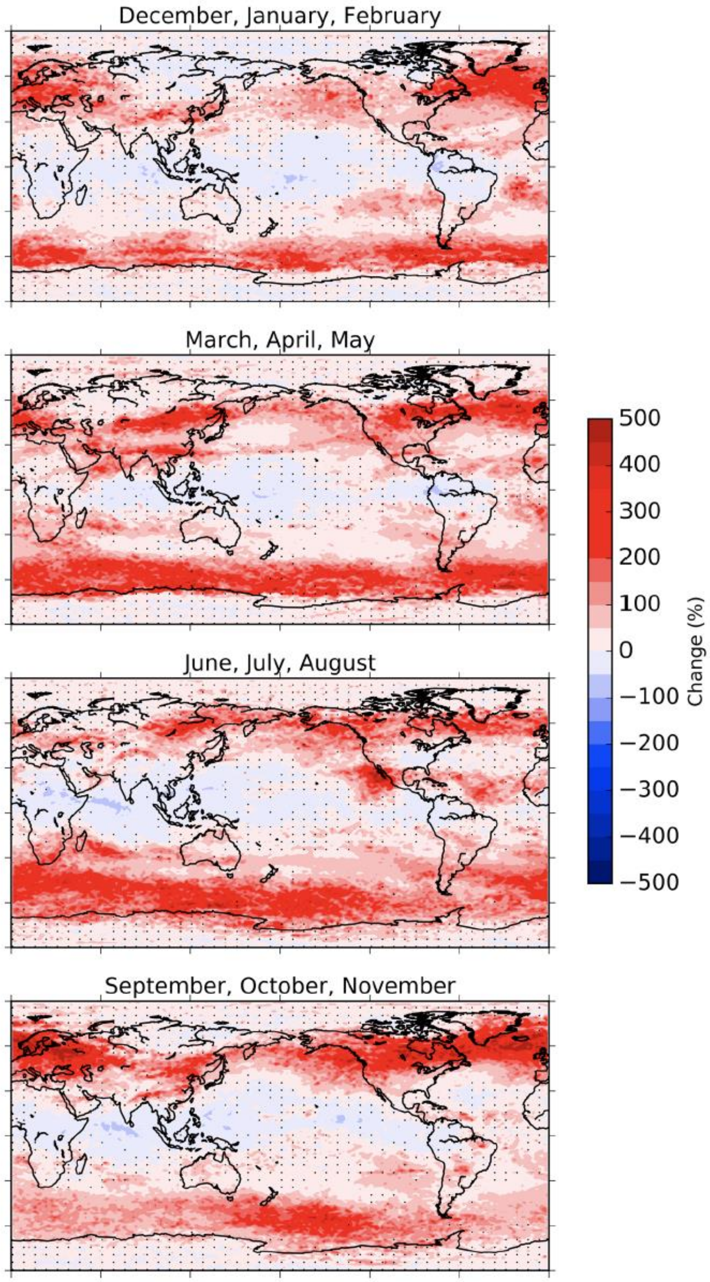

Figure B.9. Maps of the average percentage change in the amount of moderate CAT from preindustrial times (picontrol) to the period 2050–2080 (RCP8.5) at 200 hPa in each season. The average of the over all 20 CAT diagnostics, which are equally weighted [27].

Figure B.9 shows the magnitude of the moderate turbulence with respect to seasonality, in addition to coverage. The averages being taken here are equally weighted, under the assumption that each of the 20 estimates of the diagnostics is equally plausible. This assumption is fair, depending on the level of details of the analysis and consequently the accuracy of expected results. To reach higher accuracy of results, the uncertainties in diagnostic indices cannot be neglected. The skill of the diagnostics is in fact not the same for all indices. Considering set of diagnostics or weighted average of set of diagnostics, instead of simple average, that have better skills seems to be the most correct approach [8]. The skill of a diagnostic is higher if there is higher agreement with observation data. Weighted linear combinations of the clear-air turbulence diagnostics calculated from numerical weather prediction models have been found to have significant skill when verified against pilot reports (PIREPs), and these combinations are currently being used for operational turbulence predictions [8], [9].

The percentage changes generally display relatively little seasonality, with the bulk spatial patterns occurring in all four seasons, although there does appear to be a moderate seasonal amplitude modulation locally in some regions. These bulk changes include large increases of several hundred per cent in the mid-latitudes in both hemispheres. In the Southern Hemisphere, these increases peak at around 45–75° S independently of longitude. In the Northern Hemisphere, the increases peak at around 45–75° N but they display more zonal variability, which appears to be associated with the presence of land masses. The bulk features also include small and statistically insignificant decreases of several tens of per cent in parts of the tropics (where convection is a more important source of turbulence and CAT is less relevant). The global-mean percentage changes in moderate CAT at 200 hPa are +30.8% (DJF), +46.5% (MAM), +42.7% (JJA), and +39.2% (SON), where large increases in the mid-latitudes are being partly offset by small decreases in the tropics.

Table B.3. Annual-Mean Percentage Changes in the Amount of CAT From Pre-Industrial Times (picontrol) for the Period 2050–2080 (RCP8.5) [73]

Annual-Mean Percentage Changes in the Amount of CAT From Pre-Industrial Times (picontrol) to the Period 2050–2080 (RCP8.5)

Strength	North Atlantic		North America		North Pacific		Europe	
Category	200 hPa	250 hPa	200 hPa	250 hPa	200 hPa	250 hPa	200 hPa	250 hPa
Light	+75.4	+47.3	+110.1	+71.0	+120.7	+82.0	+90.5	+59.9
Light-to-moderate	+124.1	+80.7	+113.6	+57.5	+106.6	+53.8	+130.7	+75.8
Moderate	+143.3	+74.4	+100.3	+50.2	+90.2	+41.6	+126.8	+60.8
Moderate-to-severe	+148.9	+71.0	+94.3	+47.0	+73.1	+35.3	+142.1	+66.1
Severe	+181.4	+88.0	+112.7	+58.9	+91.6	+40.1	+160.7	+90.6

Strength	South America		Africa		Asia		Australia	
Category	200 hPa	250 hPa	200 hPa	250 hPa	200 hPa	250 hPa	200 hPa	250 hPa
Light	+18.3	+13.4	+24.2	+18.9	+102.5	+65.1	+18.0	+9.5
Light-to-moderate	+27.1	+18.0	+27.9	+23.3	+92.4	+48.7	+23.1	+12.9
Moderate	+34.3	+22.8	+34.3	+26.0	+78.1	+48.7	+29.6	+19.1
Moderate-to-severe	+43.3	+23.8	+36.6	+26.9	+59.2	+47.9	+36.9	+24.8
Severe	+62.0	+31.6	+51.1	+40.2	+64.1	+55.4	+52.5	+35.4

Note. The changes are calculated for five turbulence strength categories, at two pressure altitudes, and within eight geographic regions. The changes are averaged over 20 CAT diagnostics. The geographic regions are: North Atlantic (50–75°N, 10–60°W), North America (25–75°N, 63–123°W), North Pacific (50–75°N, 145°E–123°W), Europe (35–75°N, 10°W–30°E), South America (55°S–10°N, 35–80°W), Africa (35°S–35°N, 15°W–50°E), Asia (10–75°N, 45–140°E), and Australia (12–46°S, 113–177°E).

Table B.3 tabulates the annual-mean percentage changes averaged within eight geographic regions, for all five turbulence strength categories and both pressure levels. The results indicate that the busiest international airspace around the middle and high latitudes (North Atlantic, North America, North Pacific, Europe, and Asia) experiences larger increases in CAT than the global average, with the volume of severe CAT approximately doubling at 200 hPa over North America (+112.7%), the North Pacific (+91.6%), and Europe (+160.7%). The less congested skies around the tropics (Africa, South America, and Australia) generally experience smaller increases. Whereas globally, it is light turbulence that experiences the largest relative increase, locally, it can be severe turbulence (e.g., Europe). For each strength category and geographic region, the percentage change is larger at 200 hPa (12000 m) than 250 hPa (10000 m). To provide some context to aid with the interpretation of the magnitudes of these changes, in the North Atlantic (50–75° N, 10–60° W) at 200 hPa, we find that (i) in winter, severe CAT by 2050–2080 will be as common as moderate CAT in the control period, and (ii) for a range of turbulence strengths from light to moderate-to-severe, summertime CAT by 2050–2080 will be as common as wintertime CAT in the control period.

B.2 Conclusions

The following conclusions can be drawn by the current investigations on CAT:

- *the accuracy of predictability in time and space*. Results reveal that in the tropical regions (30°S–30°N), there is less agreement between the diagnostics, while in the middle and high-latitude regions, there is more agreement between the diagnostics, because CAT diagnostics were developed to diagnose and predict mid-latitude CAT near jet streams, so they are optimised to be skillful for these regions rather than the tropics. The accuracy of results therefore appears to be higher in the middle and high-latitude regions than in the tropical regions. To reach higher accuracy of results the uncertainties in diagnostic indices cannot be neglected. The skill of the diagnostics is in fact not the same for all indices. Considering specific set of diagnostics, particularly weighted average of set of diagnostics, instead of simple average, seems to be the most correct approach to increase accuracy of results [8]. Weighted average allows in fact to make more skillful diagnostics count more. The skill of a diagnostic is higher if there is higher agreement with observation data. Weighted linear combinations of the clear-air turbulence diagnostics calculated from numerical weather prediction models have been found to have significant skill when verified against pilot reports (PIREPs), and these combinations are currently being used for operational turbulence forecasting [8].

- *The seasonality*. The percentage changes generally display relatively little seasonality, with the bulk spatial patterns occurring in all four seasons, although there does appear to be a moderate seasonal amplitude modulation locally in some regions. These bulk changes include large increases of several hundred per cent of amount of CAT in the mid-latitudes in both hemispheres. In the Southern Hemisphere, these increases peak at around 45–75° S, while in the Northern Hemisphere, the increases peak at around 45–75° N but they display more zonal variability, which appears to be associated with the presence of land masses.

- *The hazard magnitude (intensity and duration)*. The busiest international airspace around the middle and high latitudes (North Atlantic, North America, North Pacific, Europe, and Asia) experiences larger increases in CAT than the global average, with the volume of severe CAT approximately doubling at 200 hPa (12000 m) over North America (+112.7%), the North Pacific (+91.6%), and Europe (+160.7%). The less congested skies around the tropics (Africa, South America, and Australia) generally experience smaller increases. Whereas globally, it is light turbulence that experiences the largest relative increase, locally, it can be severe turbulence (e.g., Europe). For each strength category and geographic region, the percentage change is larger at 200 hPa (12000 m) than 250 hPa (10000 m).

- *The hazard frequency*. In the North Atlantic (50–75° N, 10–60° W) at 200 hPa, results reveal that (i) in winter, severe CAT by 2050–2080 will be as common as moderate CAT in the control period, and (ii) for a range of turbulence strengths from light to moderate-to-severe, summertime CAT by 2050–2080 will be as common as wintertime CAT in the control period.

- *The geographical coverage*. The geographical coverage is complete. Results reveal that in the tropical regions (30°S–30°N), the percentage changes are generally smaller, while in the middle and high-latitude regions, the percentage changes are generally larger.

- The time coverage (within or beyond typical lifecycles of airplanes and runway pavements). Time coverage spans 30 years (2050-2080).

- The reliability of models. The comparison between the results of the HadGEM2-ES simulations from [27] with the GFDL-CM2.1 simulations from [29] shows for the first time that the projected increase in transatlantic turbulence is robust: it occurs across multiple climate models and it does not depend on the parameterized physics, model resolution, or greenhouse gas scenario. More research teams, e.g. CERFACS (Climate modeling and Global change Team, GLOBC), are currently working on the same topic. The future outcomes of their researches, exploiting different methodologies and climate models, may consolidate the present results.

- *Uncertainties*. Uncertainties of current investigations are listed hereafter:
  - uncertainties in diagnostic indices do exist as diagnostics do not have all the same skills. The skill of a diagnostic is higher if there is higher agreement with observation data. Weighted average of diagnostics that have better skills can reduce the uncertainties.

- Future emissions of greenhouse gases depend on socioeconomic and political factors. The corresponding uncertainty in CAT should be quantified by using other forcing scenarios in addition to the RCP8.5 scenario [30].
- The jet streams in the upper troposphere and lower stratosphere in different climate models may respond differently to a given radiative forcing anomaly dependent of the parameterization scheme selected in the models.
- Moreover, the uncertainty in CAT shall be quantified by using other climate models, such as the next generation of CMIP6 models that will have substantially higher spatial resolutions.

- *Limitations*. Limitations of current investigations are listed hereafter:
  - only 200 hPa and 250 hPa, corresponding to 10000-12000 m of altitude have been investigated. Lower and higher altitudes to cover a wider range of civil passenger aircraft may be of interest in future analyses. Moreover, the current typical cruise altitudes of medium-large subsonic civil passenger aircraft of 10000-12000 m may also change in the future, depending on the rise of the tropopause and consequently the rise of the jet streams due to an increasingly warming environment, notwithstanding the optimal aircraft performance and the propulsive technology requirements.
  - Present results do not generally include all possible sources of CAT.

B.3 Bibliography

[1]	Shine, K. P., and Coauthors, 2003: A comparison of model- simulated trends in stratospheric temperatures. Quart. J. Roy. Meteor. Soc., 129, 1565–1588.
[2]	Delcambre, S. C., D. J. Lorenz, D. J. Vimont, and J. E. Martin, 2013: Diagnosing northern hemisphere jet portrayal in 17 CMIP3 global climate models: Twenty-first-century projec- tions. J. Climate, 26, 4930–4946.
[3]	Goessling, H. F., and S. Bathiany, 2016: Why CO2 cools the mid- dle atmosphere—A consolidating model perspective. Earth System Dynamics, 7, 697–715.
[4]	Lee S.H., Williams P.D., Frame T.H., Increased shear in the North Atlantic upper-level jet stream over the past four decades (2019) Nature, 572 (7771), pp. 639 - 642. DOI: 10.1038/s41586-019-1465-z

[5]	Dutton, J., and H. A. Panofsky, 1970: Clear air turbulence: A mystery may be unfolding. Science, 167, 937–944.
[6]	Tung, K. K., and W. W. Orlando, 2003: The *k*-3 and *k*-5/3 energy spectrum of atmospheric turbulence: Quasigeostrophic two- level model simulation. *J. Atmos. Sci.,* 60, 824–835.
[7]	Koshyk, J. N., and K. Hamilton, 2001: The horizontal energy spectrum and spectral budget simulated by a high-resolution tro- posphere–stratosphere–mesosphere GCM. *J. Atmos. Sci.,* 58, 329–348.
[8]	Sharman, R., C. Tebaldi, G. Wiener, and J. Wolff, 2006: An integrated approach to mid- and upper-level turbulence forecasting. Wea. Forecasting, 21, 268–287.
[9]	Lane, T. P., R. D. Sharman, S. B. Trier, R. G. Fovell, and J. K. Williams, 2012: Recent advances in the understanding of near-cloud turbulence. Bull. Amer. Meteor. Soc., 93, 499–515.
[10]	Ellrod, Gary P., Knox, John A., Improvements to an operational clear-air turbulence diagnostic index by addition of a divergence trend term, (2010) Weather and Forecasting, 25 (2), pp. 789 - 798, DOI: 10.1175/2009WAF2222290.1
[11]	Ellrod, G. P., and D. L. Knapp, 1992: An objective clear-air turbulence forecasting technique: Verification and operational use. Wea. Forecasting, 7, 150–165.
[12]	Colson, D., and H. A. Panofsky, 1965: An index of clear-air turbulence. *Quart. J. Roy. Meteor. Soc.,* 91, 507–513.
[13]	Roach, W.T.. On the Influence of synoptic development on the production of High Level Turbulence. Quart. J. Roy. Meteor. Soc./ 96, 413-429 (1970)
[14]	MacCready, P. B (1964). Standardization of gustiness values from aircraft. *Journal of Applied Meteorology*, *3*(4), 439–449.
[15]	Williams, P. D. (2017). Increased light, moderate, and severe clear-air turbulence in response to climate change. *Advances in Atmospheric Sciences*, *34*(5), 576–586.
[16]	Williams, J. K., 2014: Using random forests to diagnose aviation turbulence. *Machine Learning*, 95, 51–70.

[17]	Schwartz, B., 1996: The quantitative use of PIREPs in developing aviation weather guidance products. Wea. Forecasting, 11, 372–384.
[18]	Kim, J.-H., and H.-Y. Chun, 2011: Statistics and possible sources of aviation turbulence over South Korea. *J. Appl. Meteor. Climatol.*, 50, 311–324.
[19]	Sharman, R. D., L. B. Cornman, G. Meymaris, J. Pearson, and T. Farrar, 2014: Description and derived climatologies of automated in situ eddy-dissipation-rate reports of atmospheric turbulence. *J. Appl. Meteor. Climatol.*, 53, 1416–1432.
[20]	Kim, B., and Coauthors, (2005) System for assessing Aviation's Global Emissions (SAGE), Version 1.5, Technical Manual FAA-EE-2005-01, Federal Aviation Administration, Washington, DC.
[21]	Malwitz, A., and Coauthors, (2005) System for assessing Aviation's Global Emissions (SAGE), Version 1.5, Validation Assessment, Model Assumptions and Uncertainties. Tech. Rep. FAA-AA-EE-2005-03, Federal Aviation Administration, Washington, DC
[22]	Wilkerson, J. T., M. Z. Jacobson, A. Malwitz, S. Balasubramanian, R. Wayson, G. Fleming, A. D. Naiman, and S. K. Lele, 2010: Analysis of emission data from global commercial aviation: 2004 and 2006. *Atmos. Chem. Phys.*, 10, 6391–6408.
[23]	Wilcox, L. J., K. P. Shine, and B. J. Hoskins, 2012: Radiative forcing due to aviation water vapour emissions. *Atmos. Environ.*, 63, 1–13.
[24]	Jaeger, E. B., and M. Sprenger, (2007) A Northern Hemispheric climatology of indices for clear air turbulence in the tropopause region derived from ERA40 reanalysis data. *J. Geophys. Res.*, 112(D20), D20106.
[25]	IPCC, 2021: Summary for Policymakers. In: Climate Change 2021: The Physical Science Basis. Contribution of Working Group I to the Sixth Assessment Report of the Intergovernmental Panel on Climate Change [Masson-Delmotte, V., P. Zhai, A. Pirani, S.L. Connors, C. Péan, S. Berger, N. Caud, Y. Chen, L. Goldfarb, M.I. Gomis, M. Huang, K. Leitzell, E. Lonnoy, J.B.R. Matthews, T.K. Maycock, T. Waterfield, O. Yelekçi, R. Yu, and B. Zhou (eds.)]. Cambridge University Press, Cambridge, United Kingdom and New York, NY, USA, pp. 3−32, doi:10.1017/9781009157896.001.
[26]	Abram, N., J.-P. Gattuso, A. Prakash, L. Cheng, M.P. Chidichimo, S. Crate, H. Enomoto, M. Garschagen, N. Gruber, S. Harper, E. Holland, R.M. Kudela, J. Rice, K. Steffen, and K. von Schuckmann, 2019: Framing and Context of the Report Supplementary Material. In: *IPCC Special Report on the Ocean and Cryosphere in a Changing Climate* [H.-O. Pörtner, D.C. Roberts, V. Masson-

	Delmotte, P. Zhai, M. Tignor, E. Poloczanska, K. Mintenbeck, A. Alegría, M. Nicolai, A. Okem, J. Petzold, B. Rama, N.M. Weyer (eds.)].
[27]	Storer, L. N., Williams, P. D., & Joshi, M. M. (2017). Global response of clear-air turbulence to climate change. Geophysical Research Letters, 44, 9976–9984. https://doi.org/10.1002/2017GL074618
[28]	Taylor, K. E., Stouffer, R. J., & Meehl, G. A (2012). An overview of CMIP5 and the experiment design. *Bulletin of the American Meteorological Society*, *93*(4), 485–498.
[29]	Williams, P. D., and M. M. Joshi, (2013) Intensification of winter transatlantic aviation turbulence in response to climate change. *Nature Clim. Change*, 3, 644–648.
[30]	Flato, G., Marotzke, J., Abiodun, B., Braconnot, P., Chou, S. C., Collins, W. J., ... Rummukainen, M. (2013). Evaluation of climate models. In T. F. Stocker et al. (Eds.), *Climate Change 2013: The Physical Science Basis. Contribution of Working Group I to the Fifth Assessment Report of the Intergovernmental Panel on Climate Change* (pp. 741–866). Cambridge, UK: Cambridge University Press.
[31]	Van Vuuren, D. P., Edmonds, J., Kainuma, M., Riahi, K., Thomson, A., Hibbard, K., ... Rose, S. K. (2011). The representative concentration pathways: An overview. *Climatic Change*, *109*, 5–31.

C Appendix AI Task Force – Level 2 AI use case description – “Proxima” virtual assistant

C.1 Proxima Overview

Proxima is a system classified as Level 2 AI-based system.

In Single Pilot Operation aircraft, Proxima and the pilot will share tasks and will have a common set of goals. Through perception and analysis, Proxima will learn from the situations encountered and will be able to continually adapt to the current situation to assist the crew in its decision-making process. Proxima will also have the ability to respond appropriately to displayed information. Proxima will also identify any mismatch between information Proxima has that is relevant to a pilot's decision and the information available to the pilot via displays and other means. It will then respond appropriately.

Proxima can:

- Follow pilot activities and displayed information and adjust its support level in view of those activities and the displayed information
- Assess the mental and physical state of the human pilot through sensors and cameras to some degree
- Detect human pilot workload, incapacitation, and make correlation between the situation and the human pilot states to adapt its level of support.
- Monitor human communications and data link with the ground and aircraft position to ensure appropriate flight path management and intervene where appropriate.

C.2 Proxima’s detailed capabilities

C.2.1 Detection of mental and physical states of the human pilot

The system will be able through sensors and cameras to have a live assessment of the mental and physical status of the human pilot.

- Proxima will have the capacity to detect workload and stress via physiological aspects such as brain and heart activity, incapacitation, fatigue to a certain degree.
- Proxima will have the capacity to make correlations between the situation and the human pilot’s states to adapt its level of support.

C.2.2. Types of interfaces Proxima can use to understand pilot and aircraft states and behaviour

User interface	HMI	Proxima		
		Reception	Output	AI Capabilities
Speech interface	Speech input	Language recognition Speech recognition	Natural Language Procedural language	- Conversational - Questions/Answers - Argumentation / Negotiation - Follow-up questions - Corrections - Explanations - Acknowledgements
Gesture interface	Spatial hands gesture Head movements User behaviour (movement, posture)	Cameras Sensors	appropriate action	Gesture recognition combined with natural language understanding
Visual interface	Displays, HW/SW	Multiple representations	Visual	TBD
Contact interface Galvanic Response	Keyboard CCD Touchscreens Skin contact with a/c controls	Conventional hardware systems 'Sweat' rate – skin conductivity	Haptic information	Pilot state detection
Haptic	Control column, throttle leavers, switches etc &	Monitoring of force, grip strength, speed etc. used when activating controls	Aural warning	Pilot state monitoring
Facial expression interface	Emotions Lips movements Pupil diameter Blink rate/duration	Cameras Eye-tracking	appropriate action	Pilot State detection Workload detection/fatigue

Neural computer interface	Brain activity signals Heart activity signals	Receptors	Control Actuations	Workload detection
Aural interface	Aural -	Voice comms – Ground Air, Air Ground	Voice comms air to ground	a/c state intervention
Interlocution	A/C signals	Computer internal business	Natural language	Prewarning of a/c status
Eye tracking	Gaze position – eye tracker	Eye fixation points	Colocation of displayed information – Synoptic screens	Interpretation of information requirements

C.3 Summary of the scenario (To be further developed)

C.3.1 Intent of the scenarios

The objective of the scenarios was to create situations where the pilot will be busy flying manually. It was anticipated as a mean to foster pilot's mental representation of the HAI with Proxima

An evolution of the roles/tasks allocation (four main subparts: Fly, Navigate, Communicate, Management of systems) is proposed to trigger some additional feedback and views:

1. Proxima capable of performing automatic configuration of the aircraft including gear extension.
2. Proxima in charge of the Navigation (FMS inputs)
3. Proxima in charge of the Communication
4. Proxima in charge of identification and management of failure.

C.3.2 Aircraft SPO, automated flight control system failure and AP loss

The scenario takes place in a flight from Paris Charles De Gaulle to Frankfurt. Pilot will be flying a commercial aircraft under SPO and acts as a Pilot In Control (PIC). The scenario starts in the air FL100 in descent. The pilot is performing the approach UNOKO 25N arrival followed by an ILS APPR to RWY 25R in navigating with the flight management system (FMS).

During the approach, the aircraft will experience a failure of the automated flight control system leading to a disengagement and loss of Autopilot in addition with a flight control failure that requires constant input of PIC flying manually. Pilot will decide to continue the approach manually up to landing. Proxima will monitor aircraft parameters, the still functioning FMS, as well as pilot states and any deviation (ref. 1.3.4 for additional use cases).

- Options for more stress: Hold instruction cancelled and instructions to intercept ILS + a/c technical failure
- Severe weather (AP disengagement)

C.3.3 Other possible scenarios for consideration

- Scenario in 1.3.2 takes place in cruise including preparation of the cabin for descent transition from cruise through the TMA and onto finals
- Severe weather (AP disengagement)
- Engine failure at take-off / in-flight
- TCAS & Avoiding action during TMA transition
- Runway change & climb restriction / level cap received during Taxi
- Proxima detects pilot drowsiness in cruise /too high level stress on approach
- Hold instruction cancelled and instructions to intercept ILS + a/c technical failure
- Oceanic clearance negotiation & transition to oceanic airspace + position reporting (+turn back if you want an emergency)
- In Cruise – cabin depressurisation requiring emergency descent
- Pilot develops health issue and is rendered incapable during final approach (transition) (Level 3?)
- Due to bad weather on approach Random aircraft (lost) is crossing ILS, high comms and monitoring w/l in addition anti-icing required
- Detection of high risk flight scenario developing – aircraft 3 rotations after maintenance, established on ILS, pilot at the end of shift pattern, bad weather & surface contamination at the airport, headwinds during flight & approaching low fuel situation.

C.3.4 Task Sharing ideas applicable to each scenario

# Use case	Task Sharing	Checklists	Crosscheck of actions	Possible HMT interaction
#1	- PIC in charge of Aviate, and Navigating and Communication tasks - Proxima in charge of managing system, and monitors PIC actions.	- Proxima will present the items - PIC will make the appropriate action	- PIC will designate the control - Proxima will provide confirmation - PIC will perform the action on the confirmed control.	Dialogue using multimodal interaction: Proxima: auditory, visual, haptic information, natural language, PIC: Voice, touch, body gesture
#2	- Proxima in charge of identification and management of failure, A/C systems, navigating. PIC : aviate, communicate	Proxima will inform PIC of failure and steps to manage PIC will confirm, may ask for explanations	Proxima will designate and perform the control PIC will provide confirmation	Proxima: informing via language PIC: Confirm with gesture or language Explanation with NLP (screens out)
#3	Proxima in charge of communication, navigating, A/C systems PIC in charge of aviating.	Proxima will use procedural / natural language for ATC and pilot interaction Reliability crucial	No cross check/monitoring of communication PIC may intervene if Proxima asks for it. PIC may ask to take back control for some tasks	Proxima expertise in procedural/ natural language, also visual haptic and auditory information PIC: body gesture and sensor data, possible conversational input